Title: Senataxin and RNase H2 act redundantly to suppress genome instability during class switch recombination

Hongchang Zhao, Krishni Satchi, Tracy Zhao and Jacqueline Barlow^†

Department of Microbiology and Molecular Genetics

*Department of Molecular and Cellular Biology

^and Genome Center

University of California, Davis

Davis CA 95616

†Corresponding author: Jacqueline Barlow, jhbarlow@ucdavis.edu

Abstract

Class switch recombination generates antibody distinct isotypes critical to a robust adaptive immune system and defects are associated with auto-immune disorders and lymphomagenesis. Transcription is required during class switch recombination for the formation of DNA double-strand breaks by AID, and strongly induces the formation of R loops within the immunoglobulin heavy chain locus. However, the impact of R loops on double-strand break formation and repair during class switch recombination remains unclear. Here we report that cells lacking two enzymes involved in R loop removal—Senataxin and RNase H2—exhibit increased R loop formation and genome instability at the immunoglobulin heavy chain locus without impacting germline transcription, splicing, recombination efficiency or AID recruitment at immunoglobulin loci. We propose that Senataxin acts redundantly with RNase H2 to mediate timely R loop removal, promoting efficient NHEJ-mediated repair and suppressing AID-dependent genome instability.

Introduction

Class switch recombination (CSR) is a programmed recombination event in mature B cells that generates antibodies of different isotypes, allowing for their interaction with different effector molecules. Successful CSR is a deletional rearrangement catalyzed by the formation of DNA double-strand breaks (DSBs) within the immunoglobulin heavy chain (IgH) switch regions. DSBs are formed by a series of events, initiated by the deamination of cytosine residues in single stranded DNA by activation-induced cytidine deaminase (AID) (Chaudhuri *et al*, 2003; Muramatsu *et al*, 2000; Pham *et al*, 2003; Ramiro *et al*, 2003b; Revy *et al*, 2000). The resulting U:C mismatches are processed by multiple DNA repair pathways producing mutations or single strand DNA (ssDNA) breaks (Stavnezer & Schrader, 2014). In CSR, multiple single-strand breaks on both Watson and Crick DNA strands create double-stranded breaks (DSBs) which initiate recombination between two adjacent but distinct genomic loci. In successful CSR, non-homologous end joining (NHEJ) proteins repair the DSBs by joining the two distal DNA ends, deleting the intervening DNA.

AID targeting during CSR

Transcriptional activity is necessary for the formation of single-strand DNA during CSR, and directly promotes AID recruitment to transcribing switch regions (Chaudhuri *et al.*, 2003; Ramiro *et al.*, 2003b; Zheng *et al*, 2015). AID interacts with the transcription factor Spt5 (Pavri *et al*, 2010; Stanlie *et al*, 2012). AID also associates with the ssDNA binding protein RPA (Chaudhuri *et al*, 2004; Yamane *et al*, 2011). More recently, researchers have shown that AID shows a binding preference for DNA forming G4 quadruplex structures, which are highly enriched in switch sequences (Qiao *et al*, 2017).

R loops form at switch regions during CSR

Transcription at the switch region also induces the formation of R loops in vitro and in vivo—three-stranded nucleotide structures where newly synthesized RNA re-anneals to the DNA template (Aguilera & Garcia-Muse, 2012; Daniels & Lieber, 1995; Reaban & Griffin, 1990; Yu *et al*, 2003). While R loops have long been observed at switch regions, their role in CSR remains confounding. The non-template DNA strand of R loops is single-stranded, creating an ideal substrate for AID (Pham *et al.*, 2003; Ramiro *et al*, 2003a; Sohail *et al*, 2003). R loop formation in switch regions is sequence-dependent, and positively correlates with AID deamination further suggesting that R loops promote AID recruitment (Huang *et al*, 2007). R loops are more stable in GC-rich sequences (Ginno *et al*, 2012; Kuznetsov *et al*, 2018; Stolz *et al*, 2019), and R loop formation in switch region correlates with G density (Zhang *et al*, 2014). Additionally, G clustering promotes R loop formation in cloned switch regions (Roy *et al*, 2008). Consistent with this, the ATP-dependent RNA helicase DDX1 can promote R loop formation in switch regions, promoting AID recruitment and DSB formation (Ribeiro de Almeida *et al*, 2018). Yet how R loops are resolved to promote DSB repair is less clear. Studies examining the RNA exosome indicate it promotes AID targeting to both strands of the DNA by helping remove R loops from the template strand, thereby exposing the DNA for deamination (Basu *et al*, 2011). However multiple studies have used ectopic expression of RNase H1 nuclease to reduce switch region R loops, with contradictory results. One

study found that ectopic RNase H1 expression in mouse CH12 cells or primary B cells reduces CSR to IgA or IgG1 respectively, however an earlier study also using CH12 cells observed no effect on CSR to IgA (Parsa *et al*, 2012; Wiedemann *et al*, 2016). Further, transgene-driven expression of murine RNase H1 in primary cells had no effect on CSR to any IgG isotype though somatic hypermutation was increased (Maul *et al*, 2017). Thus, the enzymes involved in switch region R loop removal and their impact on CSR remain elusive.

Here we use mouse knockout models of two key enzymes implicated in R loop removal, the helicase Senataxin (SETX) and a subunit of the heterotrimeric nuclease RNase H2, to assess the impact of defective R loop removal on DNA double-strand break repair during CSR in primary B lymphocytes (Becherel *et al*, 2013; Hiller *et al*, 2012). We found that cells lacking both SETX and RNase H2 activity (*Setx*$^{-/-}$*Rnaseh2b*$^{f/f}$) exhibit increased R loops specifically at the Sμ switch region, however loss of SETX or RNase H2B alone did not consistently increase R loops in primary B cells. This increase in R loops correlates with enhanced genome instability at the heavy chain locus, as ~10% of double-deficient B cells contain persistent IgH breaks and translocations, though there was no defect in CSR efficiency. Our data suggest that R loop removal at switch regions by a SETX/RNase H2 mechanism during class switch recombination suppresses error-prone end-joining and translocation formation at IgH.

Results

RNA:DNA hybrids are increased in *Setx*$^{-/-}$*Rnaseh2b*$^{f/f}$ cells.

To determine the effect of R loop metabolism on CSR, we generated mice lacking two enzymes involved in R loop removal, Senataxin and RNase H2. RNase H2 activity is essential for mouse embryogenesis, therefore mice harboring a conditional *Rnaseh2b* allele were crossed to CD19-Cre for B cell-specific gene deletion (*Rnaseh2b*$^{f/f}$), then crossed with mice containing a germline deletion of *Setx* (*Setx*$^{-/-}$) (Figure 1a, (Becherel *et al.*, 2013; Hiller *et al.*, 2012)). Freshly isolated splenic B cells were stimulated with LPS, IL-4 and α-RP105 to induce CSR to IgG1. 72 hours post-stimulation, genomic DNA was isolated and R loop levels were measured by dot blot probed with the RNA:DNA hybrid specific antibody S9.6 (Figure 1b). Cells lacking both SETX and RNase

H2B showed a 4-fold increase in total R loops, while loss of SETX or RNase H2B alone showed no significant change in R loop levels (Figure 1b,c). To determine if R loops were increased within the switch regions, we used DNA:RNA hybrid immunoprecipitation (DRIP) using a monoclonal antibody specific for RNA:RNA hybrids, S9.6. We found a consistent increase in R loop abundance at Sμ specifically in *Setx*$^{-/-}$*Rnaseh2b*$^{f/f}$ cells, while single mutants exhibited R loop levels similar to WT cells (Figure 1d). We also observed DRIP signal at the Sγ1 switch region, however all genotypes exhibited similar levels (Figure 1d). We conclude that SETX and RNase H2 act redundantly to remove RNA:DNA hybrids at Sμ.

To assess the impact of SETX and RNase H2B loss on an independent locus, we next examined RNA:DNA hybrid signal along the beta-actin gene locus *Actb*. By DRIP-Seq, we found the RNA:DNA hybrid footprint to be largely similar between the four genotypes (Supplementary Figure 1a). DRIP-qPCR analysis showed a significant increase in signal at the *Actb* intron 2 locus only in *Setx*$^{-/-}$*Rnaseh2b*$^{f/f}$ cells, however all other loci examined showed similar RNA:DNA hybrid levels in all genotypes examined (Supplementary Figure 1b). Of note, we also observed a trend for reduced DRIP signal in *Setx*$^{-/-}$ cells at the promoter and terminator regions. While somewhat surprising, these results are consistent with published reports showing depletion of SETX decreased R loops genome-wide including at the *ACTB* locus (Richard *et al*, 2020). Together, these results suggest that SETX and RNase H2 impact R loop levels at discrete loci.

Transcription is not increased in *Setx*$^{-/-}$*Rnaseh2b*$^{f/f}$ cells.

In human cells, the majority of R loop formation positively correlates with gene expression, suggesting that increased transcription can enhance R loop formation (Sanz *et al*, 2016). To determine if the increased level of R loops at switch regions was due to changes in transcriptional activity, we measured germline transcript levels at switch regions by RT-qPCR 72 hours post-stimulation. In response to LPS/IL-4/α-RP105, we observed similar levels of unspliced germline Sμ and Sγ1 transcripts in all four genotypes (Figure 1e). Thus, elevated transcription cannot explain the increased R loop levels at Sμ. Intriguingly, we observed a consistent decrease

in spliced Sμ transcripts specifically in *Setx*$^{-/-}$*Rnaseh2b*$^{f/f}$ cells suggesting that increased or persistent R loop formation may reduce splicing efficiency of germline transcripts specifically at Sμ (Figure 1e).

Cells lacking SETX or RNase H2 are proficient for class switch recombination.

R loop formation positively correlates with CSR, and are predicted to promote AID recruitment and DSB break formation within switch regions (Huang *et al.*, 2007; Yu *et al.*, 2003). Splicing of germline transcripts also correlates with productive CSR, therefore it is possible CSR would be reduced in *Setx*$^{-/-}$*Rnaseh2b*$^{f/f}$ cells (Hein *et al*, 1998; Marchalot *et al*, 2020). To determine if CSR levels are altered in SETX- and RNaseH2-deficient cells, we measured cell surface expression of IgG1 by flow cytometry. We found that CSR was similar to WT levels in *Setx*$^{-/-}$, *Rnaseh2b*$^{f/f}$ and *Setx*$^{-/-}$*Rnaseh2b*$^{f/f}$ cells at 72 and 96 hours post-stimulation (Figure 2a-c). Thus, the observed increase in DNA:RNA hybrid abundance by DRIP does not significantly impact CSR to IgG1 in *Setx*$^{-/-}$ *Rnaseh2b*$^{f/f}$ cells. To determine if CSR is proficient to other isotypes, we next measured CSR to IgA and IgG2b by stimulating cells with either LPS/α-RP105/TGF-β/CD40L or LPS/α-RP105/TGF-β, respectively. We found that switching to IgA and IgG2b was also at WT levels in *Setx*$^{-/-}$, *Rnaseh2b*$^{f/f}$ and *Setx*$^{-/-}$*Rnaseh2b*$^{f/f}$ cells (Figure 2d-f). Together, these results indicate that loss of SETX and RNaseH2 does not impact overall CSR efficiency.

***Setx*$^{-/-}$*Rnaseh2b*$^{f/f}$ cells have persistent unrepaired DNA damage at IgH.**

Defects in DNA repair during CSR result in genome instability at IgH visible as persistent DSBs and translocations in miotic chromosome spreads. Defects in R loop removal also correlate with increased DNA damage, therefore we tested if loss of SETX and RNase H2 increased genome instability at IgH. To measure persistent DNA damage and translocations at IgH, we performed fluorescent in situ hybridization (FISH) 72 hours post-stimulation in cells switching to IgG1. Spontaneous damage in *Setx*$^{-/-}$ and *Rnaseh2b*$^{f/f}$ cells was similar to WT, however *Setx*$^{-/-}$*Rnaseh2b*$^{f/f}$ cells harbored significant DNA damage, including chromosome fusions (Figure 3a). These results are similar to reports in budding yeast where combined loss of Sen1 and RNase H activity resulted in a synergistic increase in DNA damage (Costantino & Koshland, 2018). No IgH

breaks were observed in WT cells and were only found occasionally in *Setx*$^{-/-}$ and *Rnaseh2b*$^{f/f}$ cells (Figure 3b). However, we consistently observed IgH breaks or translocations in ~10% of *Setx*$^{-/-}$*Rnaseh2b*$^{f/f}$ cells (Figure 3c, n = 4 mice).

Mis-incorporated ribonucleotides do not contribute to IgH breaks in RNase H2-deficient cells.

In addition to cleaving RNA:DNA hybrids, RNase H2 also removes ribonucleotides (RNPs) mis-incorporated into DNA during replication (Hiller *et al.*, 2012; Reijns *et al*, 2012; Williams & Kunkel, 2014). High levels of genomic RNPs can lead to genome instability, therefore they may also contribute to the persistent DNA breaks observed at IgH. We first measured RNP incorporation by alkaline gel electrophoresis, as DNA enriched for RNPs is sensitive to alkaline hydrolysis leading to single-strand breaks (Nick McElhinny *et al*, 2010). We found that genomic DNA isolated from *Rnaseh2b*$^{f/f}$ and *Setx*$^{-/-}$*Rnaseh2b*$^{f/f}$ cells is more sensitive to alkaline treatment than DNA from WT or *Setx*$^{-/-}$ cells (Supplementary Figure 2a,b). Importantly, there was no significant increase in RNPs in *Setx*$^{-/-}$*Rnaseh2b*$^{f/f}$ cells compared to *Rnaseh2b*$^{f/f}$ alone. These results indicate that RNPs likely contribute to the total DNA damage observed in *Rnaseh2b*$^{f/f}$ and *Setx*$^{-/-}$*Rnaseh2b*$^{f/f}$ cells, but RNPs do not significantly contribute to the IgH breaks observed specifically in *Setx*$^{-/-}$*Rnaseh2b*$^{f/f}$ cells. In the absence of RNase H2, the type I topoisomerase Top1 cleaves RNPs from genomic DNA (Huang *et al*, 2017; Williams *et al*, 2013). We hypothesized that excess RNPs would render cells hypersensitive to the Top1 inhibitor CPT, leaving unrepaired breaks in mitosis. Indeed, we found that *Rnaseh2b*$^{f/f}$ and *Setx*$^{-/-}$*Rnaseh2b*$^{f/f}$ cells were sensitive to CPT treatment, showing similar levels of total genome instability (Supplementary Figure 2c). Yet CPT treatment did not increase DNA breaks at IgH in any genotype examined (Figure 3c, Supplementary Figure 2d). We conclude that RNP mis-incorporation does not substantially contribute to IgH breakage in *Setx*$^{-/-}$ *Rnaseh2b*$^{f/f}$ cells even in the presence of exogenous stress.

RNase H2 activity rescues DNA:RNA hybrid levels in stimulated B cells

It is possible that the increased DNA:RNA hybrids observed in *Setx*$^{-/-}$*Rnaseh2b*$^{f/f}$ cells arise indirectly due to changes in gene expression or chromatin accessibility earlier in B cell development, as conditional gene deletion using *CD19*^{cre} leads to 75-80% deletion in developing pre-B cells in the bone marrow (Rickert *et al*, 1997). To determine if RNase H2 activity directly contributes to R loop metabolism at IgH during B cell activation, we expressed FLAG-tagged RNASEH2B in *Setx*$^{-/-}$*Rnaseh2b*$^{f/f}$ splenic B cells by retroviral infection (Figure 4a). Re-expression of FLAG-tagged RNASEH2B suppressed RNP mis-incorporation alkaline gel electrophoresis indicating the FLAG tag did not substantially interfere with RNase H2 complex formation or its ability to recognize and cleave RNPs covalently attached to DNA (Figure 4b,c; (Chon *et al*, 2013)). We also found that RNASEH2B re-expression significantly reduced DNA:RNA hybrid signal at Sμ to levels similar to *Setx*$^{-/-}$ cells (Figure 4d). Finally, we also observed significant enrichment of RNASEH2B by ChIP at Sγ1 compared to Eμ which does not exhibit high levels of DNA:RNA hybrids (Figure 4e; FLAG vs. IgG control). RNASEH2B was also consistently enriched at Sμ relative to IgG, however this result was not significant due to inter-experiment variability. Together, these results indicate that RNase H2 activity contributes to DNA:RNA hybrid removal at IgH during CSR. We were not able to measure SETX binding to IgH as commercially available antibodies did not IP murine SETX (data not shown) and the size of *Setx* precludes expression by retroviral infection, as it encodes for a 2,646 amino acid protein.

Persistent IgH breaks and translocations are dependent on AID activity.

To determine if AID activity is required for the persistent DSBs observed at IgH, we next stimulated cells with α-RP105 alone. Stimulation with α-RP105 induces cell proliferation, however AID expression is minimal compared to stimulation also containing LPS or LPS+IL-4 (Supplementary Figure 3a-b; (Callen *et al*, 2007)). CSR to IgG1 was lower than 1% in all genotypes analyzed, correlating CSR efficiency with AID expression (Supplementary Figure 3c). Total DNA damage levels were similar to LPS/IL-4/α-RP105-stimulated cells, however we did not detect any DSBs or translocations at IgH in α-RP105-stimulated cells for any genotype (Supplementary Figure 3d, Supplementary table 1). These results indicate that the IgH damage

observed in *Setx*$^{-/-}$*Rnaseh2b*$^{f/f}$ cells was AID-dependent. Further, only *Setx*$^{-/-}$*Rnaseh2b*$^{f/f}$ cells consistently accumulate spontaneous unrepaired breaks in the absence of AID expression. It is possible that stimulation with α-RP105 alone alters transcriptional activity and R loop formation within IgH compared to stimulation with LPS/IL-4/α-RP105, altering the potential for R loop-induced IgH breaks. To confirm IgH damage was dependent on AID, we next generated *Aicda*$^{-/-}$, *Aicda*$^{-/-}$*Setx*$^{-/-}$, *Aicda*$^{-/-}$*Rnaseh2b*$^{f/f}$ and *Aicda*$^{-/-}$*Setx*$^{-/-}$*Rnaseh2b*$^{f/f}$ mice, stimulated B cells with LPS/IL-4/α-RP105 for 72 hours and performed IgH FISH on metaphase spreads. We observed no IgH breaks in LPS/IL-4/α-RP105-stimulated cells lacking AID, however *Aicda*$^{-/-}$*Setx*$^{-/-}$ *Rnaseh2b*$^{f/f}$ B cells had elevated levels of non-IgH damage (Supplementary Figure 3e,f). Importantly, 7.6% of control *Setx*$^{-/-}$*Rnaseh2b*$^{f/f}$ cells stimulated side-by-side had IgH breaks, consistent with previous experiments. Together, these results show that the persistent IgH breaks and translocations observed in *Setx*$^{-/-}$*Rnaseh2b*$^{f/f}$ cells are AID-dependent.

AID expression and recruitment to switch regions is not altered in SETX or RNase H2-deficient cells.

AID overexpression induces high levels of DSBs, increasing class switch recombination efficiency and unrepaired breaks at IgH. To determine if loss of SETX or RNase H2 affected AID expression, we first measured *Aicda* transcript levels. We found that *Aicda* transcripts were similar to WT levels in *Setx*$^{-/-}$, *Rnaseh2b*$^{f/f}$, and *Setx*$^{-/-}$*Rnaseh2b*$^{f/f}$ cells (Supplementary figure 4). AID stability is also regulated during CSR. To determine if protein levels were altered, we next measured protein abundance and found that AID expression was similar in all four genotypes (Figure 5a,b). These results show that the increased damage at IgH is not due to AID overexpression.

Enhanced recruitment of AID to switch regions positively correlates with DSB formation and CSR efficiency. To determine if AID recruitment is altered, we performed chromatin immunoprecipitation (ChIP) of AID in WT, *Setx*$^{-/-}$, *Rnaseh2b*$^{f/f}$, and *Setx*$^{-/-}$*Rnaseh2b*$^{f/f}$ cells. We found similar levels of AID recruitment at both the Sγ1 and Sμ switch regions in WT, *Setx*$^{-/-}$, *Rnaseh2b*$^{f/f}$, and *Setx*$^{-/-}$*Rnaseh2b*$^{f/f}$ cells by ChIP-qPCR (Figure 5c). All four genotypes examined showed enrichment at Sγ1 and Sμ compared to *Aicda*$^{-/-}$ cells. These results

indicate that AID targeting to chromatin is not significantly altered in *Setx*$^{-/-}$*Rnaseh2b*$^{f/f}$ cells, and enhanced AID targeting to switch regions is unlikely to be the cause of the increased IgH instability.

RNA polymerase association with switch regions is normal in SETX- and RNase H2-deficient cells.

AID physically associates with the transcription factor Spt5, leading to deamination both within and outside switch regions (Pavri *et al.*, 2010; Stanlie *et al.*, 2012). It is possible slower R loop turnover will increase the dwell time of RNA polymerase II (PolII) at R loop-forming genes. To determine if PolII association at switch regions is increased, we performed ChIP of activated PolII (PolII-S5P) in all four genotypes. We found that WT, *Setx*$^{-/-}$, *Rnaseh2b*$^{f/f}$, and *Setx*$^{-/-}$*Rnaseh2b*$^{f/f}$ cells all had similar levels of PolII-S5P at both Sμ and Sγ1 switch regions (Figure 5d). PolII ChIPs showed variability particularly in *Rnaseh2b*$^{f/f}$ cells, however IgH breaks were consistently increased *Setx*$^{-/-}$*Rnaseh2b*$^{f/f}$ cells in every experiment. Thus, we conclude that increased PolII association at switch regions is not the cause of persistent IgH DNA damage observed in *Setx*$^{-/-}$*Rnaseh2b*$^{f/f}$ cells.

Proliferation and cell cycle distribution is normal in cells lacking SETX and RNase H2B

Activated B lymphocytes proliferate extremely rapidly, potentially impacting DNA repair and genome instability (Lyons & Parish, 1994). To determine if cell proliferation is altered, we isolated resting lymphocytes, labeled them with CFSE to track cell division, and stimulated switching to IgG1. After 72 hours, we analyzed CFSE dye dilution and IgG1 expression by flow cytometry. We found that *Rnaseh2b*$^{f/f}$ and *Setx*$^{-/-}$*Rnaseh2b*$^{f/f}$ cells exhibited a modest decrease in cell proliferation (Supplementary Figure 5a). CSR frequency correlates with cell division rate(Hodgkin *et al*, 1996); however the CSR frequency was similar in all genotypes examined (Supplementary Figure 5b). It is possible that the persistent DSBs observed in *Setx*$^{-/-}$*Rnaseh2b*$^{f/f}$ cells trigger DNA damage checkpoint activation, altering cell cycle distribution. Cell cycle phase impacts DSB end resection and repair pathway choice, therefore we analyzed cell cycle profiles by PI staining (Symington, 2016). We found all genotypes had similar fractions of cells in G1, S and G2/M phases (Supplementary Figure 5c,d). Thus,

we conclude that the increase in unrepaired breaks is not due to changes in DNA repair from altered cell cycle distribution.

Discussion

Co-transcriptional R loop formation has emerged as a regulator of CSR involved in targeting AID to the appropriate switch regions for DSB formation. AID recruitment to chromatin is a highly regulated act, as off-target AID activity promotes IgH and non-IgH DSBs and translocations associated with carcinogenesis (Ramiro *et al*, 2004; Robbiani *et al*, 2008; Robbiani *et al*, 2009). However persistent R loops are also sources of replication-associated DNA damage and genome instability (Crossley *et al*, 2019; Marnef & Legube, 2021; Prado & Aguilera, 2005; Stork *et al*, 2016). Here we show that combined loss of SETX and RNase H2 leads to an increase in switch region R loop abundance and IgH damage in the form of unrepaired DSBs and translocations in mitotic cells. SETX and RNase H2 also have independent functions in DNA repair, however loss of either factor alone was not sufficient to significantly increase R loops or IgH instability. Loss of SETX and RNase H2 did not substantially alter transcription, splicing, or AID recruitment at switch regions. From this work, we propose the shared function of SETX and RNase H2 in R loop removal promotes efficient NHEJ during CSR.

Separation between CSR efficiency and IgH instability

In contrast to a prior report, we found that CSR efficiency to IgG1, IgG2B and IgA in *Setx*$^{-/-}$ and *Setx*$^{-/-}$ *Rnaseh2b*$^{f/f}$ cells was comparable to WT cells indicating the majority of DSBs created productive junctions leading to cell surface expression (Figure 2; (Kazadi *et al*, 2020)). This is consistent with our results which showed no change in germline transcription, RNAP2 association, or AID recruitment. Thus, why do *Setx*$^{-/-}$ *Rnaseh2b*$^{f/f}$ cells have substantially increased IgH breaks without a detectable reduction in CSR? To date, the vast majority of mouse models exhibiting increased IgH breaks by metaphase spread analysis also exhibit an alteration in CSR efficiency detectable by flow cytometry or ELISA. Loss of mismatch repair (MMR) factors (MLH1, PMS2, Mbd4), DSB processing factors (CtIP, Exo1), NHEJ proteins (Ku70, Ku80, Xrcc4, Lig4), mediators

(53bp1, Rnf8), or kinases (ATM, DNAPKcs) all show reduced CSR efficiency along with IgH instability (Alt *et al*, 2013; Bardwell *et al*, 2004; Boboila *et al*, 2010; Callen *et al.*, 2007; Casellas *et al*, 1998; Franco *et al*, 2008; Grigera *et al*, 2017; Gu *et al*, 1997; Lee-Theilen *et al*, 2011; Li *et al*, 2010; Lumsden *et al*, 2004; Manis *et al*, 2002; Reina-San-Martin *et al*, 2004; Santos *et al*, 2010; Schrader *et al*, 2002; Ward *et al*, 2004; Yan *et al*, 2007). Alternatively, enhanced AID expression or nuclear localization increases AID-associated instability, however this is accompanied by elevated CSR frequency (Robbiani *et al.*, 2009; Uchimura *et al*, 2011). Alt-EJ has been proposed to be a default pathway used when cNHEJ proteins are absent (Bennardo *et al*, 2008; Boboila *et al.*, 2010; Nussenzweig & Nussenzweig, 2007; Soulas-Sprauel *et al*, 2007; Stavnezer & Schrader, 2014; Yan *et al.*, 2007), however we report a scenario where unrepaired breaks are increased without a concomitant reduction in CSR suggesting that repair efficiency is reduced even when all core cNHEJ factors are present. This is not without precedent, as cells lacking the nuclease Artemis exhibit increased MH use at switch junctions without substantially affecting CSR to most isotypes (Du *et al*, 2008; Rivera-Munoz *et al*, 2009). Taken together, these results indicate that DSB formation and DNA end joining processes are largely intact in *Setx*$^{-/-}$*Rnaseh2b*$^{f/f}$ cells, however NHEJ efficiency is likely impaired.

Efficient R loop removal promotes cNHEJ and genome integrity during CSR.

We propose that an increased persistence of R loops at switch regions interferes with DSB end processing and joining, resulting in the IgH instability observed in *Setx*$^{-/-}$*Rnaseh2b*$^{f/f}$ cells (Figure 3b,c). This places SETX and RNase H2 downstream of DDX1, an RNA helicase which promotes R loop formation and AID targeting by unwinding G4 quadruplex structures in switch transcripts (Ribeiro de Almeida *et al.*, 2018). Normally, SETX and RNase H2 remove switch R loops along the non-template strand, exposing ssDNA to AID-dependent deamination and the formation of “clean” DSB ends appropriate for cNHEJ (Figure 6a). In the absence of SETX and RNase H2, R loops persist along the switch regions (Figure 6b). This potentially affects CSR in two distinct ways—by changing the type of DSBs created, or by interfering with DSB repair protein recruitment. In the first possibility, persistent RNA:DNA hybrids could block AID access to the template strand, increasing the length of

5’ ssDNA tails at DSB ends (Figure 6b). This model is supported by a potential role of the RNA exosome in CSR where AID association with RNA exosome components promotes deamination on both template and non-template DNA strands, presumably by removing RNA annealed to the template strand (Basu *et al.*, 2011). Persistent R loops may block AID binding to ssDNA, generating DSB ends with 3’ or 5’ ssDNA tails that would require end filling or cleavage to produce blunt DSB end substrates for cNHEJ. Long ssDNA tails containing short stretches of MH can also anneal to one another, shunting repair towards alt-EJ (Alt *et al.*, 2013; So & Martin, 2019; Stavnezer & Schrader, 2014). Annealed ssDNA tails would also likely require trimming prior to ligation. In support of this notion, loss of Artemis increases the frequency of unrepaired IgH breaks and MH use at switch junctions (Du *et al.*, 2008; Franco *et al.*, 2008; Rivera-Munoz *et al.*, 2009).

Alternatively, efficient R loop removal may be necessary after DSB formation to promote efficient repair by NHEJ. Here, persistent RNA:DNA hybrids at or near DSB ends could interfere with efficient repair by protecting ssDNA overhangs from processing or by blocking cNHEJ protein binding to DSB ends. Most DSB ends can undergo trimming yielding substrates with short < 3 bp overhangs, suitable for cNHEJ. The Ku70/Ku80 heterodimer has lyase activity, preferentially removing apurinic/apyridimic (AP) nucleotides from the 5’ end of DSBs (5’-dRP) (Roberts *et al*, 2010). This activity appears restricted to short 5’ overhangs, potentially lessening its interference with HR-mediated repair requiring long 3’ssDNA tails (Strande *et al*, 2012; Symington, 2016). Artemis also promotes NHEJ and suppresses IgH damage (Chang *et al*, 2016; Chang *et al*, 2017; Franco *et al.*, 2008). R loop removal also appears important for later steps of HR; blocking their removal by SETX depletion does not impair DSB end resection, but does slow the recruitment of the strand invasion factor Rad51 (Cohen *et al*, 2018).

These two models of how R loops impact CSR are not mutually exclusive, as the type of DSB ends created directly affects repair protein binding affinity, and which proteins are necessary for successful repair (Chang *et al.*, 2017; Serrano-Benitez *et al*, 2019; Symington, 2016). We propose that persistent R loops promote the formation of long (> 6 bp) ssDNA tails, increasing the frequency of error-prone EJ at switch joins in *Setx*$^{-/-}$, *Rnaseh2b*$^{f/f}$, and *Setx*$^{-/-}$*Rnaseh2b*$^{f/f}$ cells. In the absence of both SETX and RNase H2, RNA:DNA hybrids

persist at a subset of DSB ends, interfering with efficient repair and leading to persistent IgH breaks and translocations in mitosis. However, many enzymes—including the RNA exosome, RNase H1, and additional RNA:DNA-specific helicases—can also remove these structures indicating the resolution step of CSR is slowed but not blocked. Indeed, Senataxin is not unique in its ability to unwind RNA:DNA hybrids, therefore additional R loop resolving enzymes may also influence CSR. Multiple helicases have been implicated in R loop removal associated with replication stress including Aquarius, DDX19, and DDX21, among others (Hodroj *et al*, 2017; Sollier *et al*, 2014; Song *et al*, 2017). It will be interesting to determine if these enzymes exhibit similar or distinct effects on CSR.

Materials and Methods

Mice

Setx$^{-/-}$, *Rnaseh2b*$^{f/f}$, and *CD19*^{cre} mice were previously described and used to generate *Setx*$^{-/-}$ *Rnaseh2b*$^{f/f}$ *CD19*^{cre} mice (Becherel *et al.*, 2013; Hiller *et al.*, 2012; Rickert *et al.*, 1997). For CSR to IgG1, we used a minimum of 10 mice per genotype to reach a power of 0.8 with an expectation to see a 25% difference. A priori power calculations to determine mouse numbers were based on reported CSR data from (Kazadi *et al.*, 2020) and performed using G*power 3.1. Since no difference in CSR was detected for IgG1, subsequent CSR studies were based on similar reports in the literature, using a minimum of n=4 mice per genotype. For molecular analyses, we used n=3 mice to reach a power of 80% for p value calculations estimating differences to be consistently 50% or greater. Primary cells from both male and female mice were used to eliminate sex bias. No difference was observed between sexes. The age of mice was matched in experiments to reduce bias, as this variable is known to alter DNA repair efficiency and CSR. No randomization or blinding was used in mouse experiments. All mouse experiments were performed in accordance with protocols approved by the UC Davis Institutional Animal Care and Use Committee (IACUC protocol #20042).

B cell stimulation

CD43^{-} resting B cells were isolated using the Dynabeads untouched CD43 mouse B cell isolation kit (Thermo Fisher, 11422D). Isolated B cells were cultured in B cell media (BCM, RPMI-1640 supplemented with 10% fetal calf serum, 1% L-glutamine, 50 IU/ml penicillin/streptomycin, 1% sodium pyruvate, 53 µM 2-mercaptoethanol, 10 mM HEPES). B cells were stimulated with LPS, α-RP105 and interleukin 4 (IL-4) for IgG1, LPS/α-RP105/TGF-B for IgG2b and LPS/α-RP105/TGF-B/CD40L for IgA class switch recombination.

DRIP analyses (dot blot, qPCR)

DRIP was performed as described (Sanz *et al.*, 2016). Briefly, after gentle genomic extraction and restriction enzyme cocktail (HindIII, XbaI, EcoR1, Ssp1, BrsG1) fragmentation, 4 micrograms of digested DNA in DRIP

buffer (10mM NaPO4 pH 7.0 140mM NaCl 0.05% Triton X-100) were incubated with 2 micrograms of S9.6 antibody overnight at 4 ℃, In-vitro RNase H treated sample was used as negative control. After antibody DNA complexes were bound to Protein G Dynabeads and thoroughly washed, DNA was recovered with Chelex-100, the bound fraction was suspended in 0.1 ml 10% Chelex-100 (Bio-Rad), vortexed, boiled for 10 min, and cooled to room temperature. This sample was added to 4µl of 20 mg/ml Proteinase K followed by incubation at 55°C for 30 min while shaking. Beads were boiled for another 10 min. Sample was centrifuged and supernatant collected. Beads were suspended with 100 µl 2× TE to the beads, vortexed, centrifuged, and supernatants pooled. qPCR was performed with SYBR Select Master Mix (thermo fisher) and analyzed on a Light Cycler 480 (Roche), enrichment calculated by ratio of DRIP/input.

For dot blot analysis, fragmented genomic DNA was spotted in serial 2-fold dilutions and loaded onto a dot blot device assembled with Whatman paper and nitrocellulose membrane. The membrane was crosslinked in UV-crosslinker 120000uJ/cm2 for 15s, blocked with odyssey TBST blocking buffer, and incubated with the anti-DNA–RNA hybrid S9.6 antibody overnight at 4°C. Goat anti-mouse AlexaFluor 680 secondary antibody (A21057) was used. Quantification on scanned image of blot was performed using ImageJ Lab software.

Real time quantitative RT-PCR

Total RNA was extracted from stimulated primary B cells with TRIzol (Invitrogen), followed by reverse transcription with ProtoScript II First Strand cDNA Synthesis Kit (NEB) according to the manufacturer's protocol. qPCR was performed using SYBR Select Master Mix (thermo fisher) and analyzed on a Light Cycler 480 (Roche). Gene of interest/ normalizing gene values ± SD were then normalized to the WT controls; Germline switch region transcription value were normalized to CD79b transcripts before normalized to the WT control. Primers are listed in supplementary table 2.

Flow cytometry

Primary B cells were washed with PBS and stained with B220-FITC and biotin anti-IgG1 (BD), biotin anti-IgG2b (BioLegend), PE anti-IgA (SouthernBiotech). For biotinylated primary antibodies, cells were then stained with PE-Streptavidin (Beckman Coulter). Data were collected on a BD FACSCanto™ and analyzed using FlowJo software. At least 20,000 events of live lymphoid cells were recorded. For CFSE staining, freshly isolated primary B cells were washed and resuspended in 0.1% BSA/PBS at 1 x 10^7 cells/ml and labeled with CFSE at a final concentration of 5uM for 10 min at 37°C. CFSE was quenched with ice-cold RPMI 1640 medium containing 10% FCS and washed twice with BCM. Labeled cells were then cultured in BCM and appropriate stimuli for 72 or 96 hours days prior to analysis. For cell cycle analysis, B cells were harvested 72 hours post-stimulation, washed once with PBS and resuspended in ice-cold 70% ethanol while slowly vertexing. Cells were fixed overnight, then washed with PBS one time. Cell pellets were resuspended in propidium iodide (PI) staining solution (50 µg/ml PI and 100 units/ml RNase A in PBS), then incubated at room temperature in the dark for 2 hours. Fifty-thousand gated events were collected on a BD FACSCanto™ and analyzed by Flowjo software.

Metaphase chromosome preparation and fluorescent in situ hybridization (FISH)

The metaphase chromosome preparation and FISH was performed as descripted (Waisertreiger *et al*, 2020). Briefly, Day3 stimulated primary B cells were arrested in metaphase by a 1-h treatment with 0.1 µg/ml demecolcine (Sigma, D1925), treated with 0.075 M KCl, fixed in methanol:acetic acid (3:1), spread onto glass slides and air-dried. FISH were performed on metaphase cells using IgH probe. Prior to hybridization, slides were briefly heated over an open flame, denaturing DNA for IgH detection. Slides were washed in 1 × PBS at room temperature (RT) for 5 min, post-fixed in 1% formaldehyde at RT for 5 min, and washed in 1 × PBS at RT for 5 min. Slides were dehydrated in ethanol (75, 85, and 100%) at RT for 2 min each and air-dried. Cells and probes were co-denatured at 75 °C for 3 min and incubated overnight at 37 °C in a humid chamber. Slides were washed post-hybridization in 0.4 × SSC/0.3% NP-40 at 72 °C (2 min), then 2 × SSC/0.1% NP-40 at RT (2 min). Slides were probed with 0.25 µM telomere probe (PNA Bio, F1002) for 1 hour at RT. Slides were then

washed in 1 × PBST (1X PBS, 0.5% Triton-X-100) for 5 min at 37 °C. After wash with PBS and dehydrated in ethanol (75, 85, and 100%), Slides were counterstained with Vectashield mounting medium containing DAPI (Vector laboratories Inc., H-1200) before microscopy.

Microscopy and analysis

B cells were isolated and cultured from a separate mouse for each experiment. A minimum of 50 metaphases were analyzed for each experiment. Metaphases images were acquired using an epifluorescent Nikon microscope with NIS Elements AR4.40.00 software (Nikon). Downstream analysis used ImageJ software (NIH).

Protein blot and immunoprecipitation

Protein expression was analyzed 72 hours post-stimulation for switching cells unless otherwise indicated. Briefly, 0.5 million cells were suspended with RIPA buffer (50 mM Tris-HCl pH8.0,150 mM NaCl, 2 mM EDTA pH8.0, 1% NP-40, 0.5% Sodium Deoxycholate, 0.1% SDS, Protease Inhibitors) and incubated at 4℃ for 30 min, following centrifuge to remove the thick DNA, the whole cell lysis was boiled in protein loading buffer for SDS-PAGE. Immunoblotting was performed with the appropriate primary and secondary antibodies. For FLAG-RNaseH2B immunoprecipitation, total cell lysates were prepared in RIPA buffer and incubated with a desired antibody and appropriate protein A/G-agarose beads at 4°C overnight with gentle agitation. Beads were washed 3 times with lysis buffer, and immunocomplexes were eluted by boiling in SDS sample buffer for 5 min before loading. Anti-AID (Thermo Fisher ZA001) at 1:500 dilution, Anti-β-Actin (Abclonal, AC026) at 1: 100000 dilution, Anti-FLAG (Abclonal, AE005), Goat anti-mouse AlexaFluor 680 secondary antibody (A21057) and Goat anti rabbit AlexaFluor 790 secondary antibodies (A11367) were employed.

ChIP

CHIP was performed as described (Barlow *et al*, 2013), Briefly, 1×10^7 stimulated primary B cells were cross-linked with 0.5% formaldehyde for 5 min, then quenched by addition of 125 mM glycine for 5 min at RT.

Crosslinked cells were washed with ice-cold PBS three times and then resuspended in ice-cold RIPA buffer (50 mM Tris-HCl pH8.0, 150 mM NaCl,2 mM EDTA pH8.0, 1% NP-40, 0.5% Sodium Deoxycholate, 0.1% SDS, Protease Inhibitors). Chromatin was sheared with a Bioruptor (Diagenode) ultrasonicator to the size range between 200-1000 bp. Samples were centrifuged and supernatant collected, 1% percent of lysate as whole cell DNA input. Antibody-coupled Dynabeads Protein G (Thermo Fisher) were used for immunoprecipitations performed overnight at 4°C. Anti-AID (Thermo Fisher ZA001), Anti-Pol ll Serine5 Phospho (4H8, AB5408) and IgG (AB37355) was used for immunoprecipitation. Beads were washed once in each of the following buffers for 10 min at 4℃: Low salt buffer (0.1% SDS 1% Triton X-100 2 mM EDTA 20 mM Tris-HCl pH 8.0 150 mM NaCl), high salt buffer (0.1% SDS 1% Triton X-100 2 mM EDTA 20 mM Tris-HCl pH 8.0 500 mM NaCl), LiCL buffer (0.25 M LiCl 1% NP-40 1% Sodium Deoxycholate 1 mM EDTA 10 mM Tris-HCl pH 8.0), and TE buffer (50 mM Tris, pH 8.0, 10 mM EDTA). DNA was recovered with Chelex-100 and analysis by qPCR. Data were analyzed using the comparative CT method. Fold enrichment was calculated as ChIP/Input. Primers used for qPCR are listed in supplementary table 2.

Alkaline gel electrophoresis

For alkaline gel electrophoresis, genomic DNA was extracted from day 3 LPS/IL4/RP105-stimulated B cells. 2ug of genomic DNA was incubated in 0.3 M NaOH for 2 hours at 55℃ and separated on an 0.9% agarose gel (50 mM NaOH, 1 mM EDTA) as previously described (Mcdonell *et al*, 1977). Gels were neutralized with neutralizing solution (1M Tris-HCL, 1.5M NaCL) and stained with ethidium bromide prior to imaging. Densitometry was analyzed with ImageJ software (NIH).

Retroviral preparation and B cell infection

Viral infection was performed as described (Waisertreiger *et al.*, 2020). After verification of infection efficiency by flow cytometry, cells were harvested for genomic DNA extraction, DRIP, immunoprecipitation-WB and FISH.

Acknowledgements

This work was supported by research funding from the National Cancer Institute K22CA188106 and a National Institute for General Medical Studies grant 1R01 GM134537 (JHB). This study utilized the University of California Davis Cancer Center Flow Cytometry core partially supported by National Institute of Health grant S100D018223. Thanks to Drs. Lionel Sanz, Stella Hartono, and Frederic Chedin for assistance with DRIP, DRIP-Seq and DRIP-qPCR assays, and to Drs. Klaus Rajewsky, Martin Lavin and Axel Roers for mouse models. We would like to thank Dr. Frederic Chedin, Lionel Sanz, Commodore St Germain and all members of the Barlow and Chedin labs for helpful discussions and suggestions, and Jack McTiernan for assistance with figure design.

Competing interests

The authors report no competing interests.

Figure legends

Figure 1. RNA-DNA hybrids are increased in *Setx*$^{-/-}$*Rnaseh2b*$^{f/f}$ B cells during CSR to IgG1.

A. Senataxin (SETX) and RNase H2 contribute to RNA:DNA hybrid removal; SETX helicase activity unwinds the nucleotide strands retaining both the RNA and DNA components while RNase H2 cleaves RNA, retaining only the DNA strand. **B.** Dot blot analysis of R-loop formation: two-fold serial dilutions of genomic DNA starting at 1 microgram were arrayed on a nitrocellulose membrane and probed using the S9.6 antibody; RNase H treatment of the *Setx*$^{-/-}$*Rnaseh2b*$^{f/f}$ sample was used as the negative control. **C.** Quantitation of 0.5 micrograms, 0.25 micrograms and 0.125 micrograms dot blot from (**B**) using imageJ; values were normalized to WT, set as 1. Figure are expressed as fold-change relative to WT. Error bars are the standard deviation between different experiments; * = $p < 0.05$ comparing different genotypes using multiple T-test (n = 3 mice/genotype). **D.** Diagram of the IgH locus showing the location of PCR products used for ChIP and DRIP assays. DRIP assay was performed with S9.6 antibody using primary B cells after 72 hours of stimulation to IgG1 with LPS/IL-4/α-RP105; RNase H treatment of *Setx*$^{-/-}$*Rnaseh2b*$^{f/f}$ sample was used as the negative control. Relative enrichment was calculated as ChIP/input and the results were replicated in three independent experiments. Error bars show standard deviation; statistical analysis was performed using one-way ANOVA (n = 3 mice/genotype). **E.** Diagram of the IgH locus showing the location of PCR products for germline transcription under IgG1 stimulation with LPS/α-RP105/IL4. Real-time RT-PCR analysis for germline transcripts (Ix-Cx) at donor and acceptor switch regions in WT, *Setx*$^{-/-}$, *Rnaseh2b*$^{f/f}$, and *Setx*$^{-/-}$ *Rnaseh2b*$^{f/f}$ splenic B lymphocytes cultured for 72 h with LPS/IL-4/α-RP105 stimulation. Expression is normalized to CD79b and is presented as relative to expression in WT cells, set as 1. Error bars show standard deviation; statistical analysis was performed using multiple t-test (n = 4 mice/genotype).

Figure 2. CSR is not reduced in *Setx*$^{-/-}$, *Rnaseh2b*$^{f/f}$ or *Setx*$^{-/-}$*Rnaseh2b*$^{f/f}$ B cells. Percentage of cells undergoing CSR to IgG1 72 hours (**A**) and 96 hours (**B**) post-stimulation with LPS/IL-4/α-RP105. **C.** Representative flow cytometry analyses of IgG1^{+} and B220 expression in response to LPS/IL-4/α-RP105. The percentage of IgG1^{+} B

cells is indicated at top left. Percentage of cells undergoing CSR to IgA (**D)** or IgG2B (**E**) 72 hours post-stimulation. **F.** Representative flow cytometry analyses of IgA^+ and B220 expression in response to LPS/α-RP105/TGF-B/CD40L. **G.** Representative flow cytometry analyses of $IgG2B^+$ and B220 expression in response to LPS/α-RP105/TGF-B. Horizontal lines in dot plots indicate mean, error bars show standard error of the mean (SEM). Statistical significance versus WT was determined by one-way ANOVA; each dot represents an independent mouse.

Figure 3. Increased IgH damage is observed in *Setx$^{-/-}$Rnaseh2b$^{f/f}$* B cells. A. Frequency of spontaneous DNA damage in WT, *Setx$^{-/-}$, Rnaseh2b$^{f/f}$* and *Setx$^{-/-}$Rnaseh2b$^{f/f}$* cells. **B.** Representative images of the types of rearrangements produced. IgH specific probe visualized in green, Telomere-specific probe visualized in red, DAPI is in blue. **C.** Frequency of spontaneous DNA damage at IgH. All cells were harvested 72 hours post-stimulation to IgG1 with LPS/IL-4/α-RP105. Error bars show standard deviation; statistical significance versus WT was determined by one-way ANOVA (n = 4 independent mice).

Figure 4. RNase H2 activity rescues DNA:RNA hybrid levels in stimulated B cells.

A. Total cell lysates were extracted from *Setx$^{-/-}$Rnaseh2b$^{f/f}$* cells stimulated for 96 hours with LPS/IL-4/α-RP105. Cells were infected with empty vector or retrovirus, expressing FLAG-RNaseH2B, then subjected to immunoprecipitation and immunoblotting with indicated antibodies. **B.** Representative image of alkaline gel from *Setx$^{-/-}$, Setx$^{-/-}$Rnaseh2b$^{f/f}$* EV and *Setx$^{-/-}$Rnaseh2b$^{f/f}$* + FLAG-RNaseH2B cells (n=3 independent mice/genotype). **B.** Densitometry trace of representative alkaline gel in (**A**). **C.** DRIP assay was performed with S9.6 antibody on *Setx$^{-/-}$, Setx$^{-/-}$Rnaseh2b$^{f/f}$* and *Setx$^{-/-}$Rnaseh2b$^{f/f}$* + FLAG-RNaseH2B-expressing cells stimulated with LPS/IL-4/α-RP105 for 96 hours. RNase H treatment of *Setx$^{-/-}$Rnaseh2b$^{f/f}$* sample was a negative control. Relative enrichment was calculated as ChIP/input and the results were replicated in three independent experiments. Error bars show standard deviation; statistical analysis was performed using one-

way ANOVA. **E.** ChIP analysis for FALG-RNaseH2B occupancy in Eμ, Sμ and Sγ regions of primary B cells in response to LPS/IL-4/α-RP105 stimulation. Relative enrichment was calculated as ChIP/input. Error bars show standard deviation. Statistical analysis was performed using student t-test (n = 3 mice/genotype).

Figure 5. AID expression and recruitment are not altered in *Setx*$^{-/-}$, *Rnaseh2b*$^{f/f}$ and *Setx*$^{-/-}$*Rnaseh2b*$^{f/f}$ B cells. **A.** AID protein expression in WT, *Setx*$^{-/-}$, *Rnaseh2b*$^{f/f}$, *Setx*$^{-/-}$*Rnaseh2b*$^{f/f}$ and *Aicda*$^{-/-}$ cells 72 hours post-stimulation to IgG1. Western blots were probed with an anti-AID antibody and anti-actin as loading control. *Aicda*$^{-/-}$ cells were used as a negative control. **B.** Quantification of AID protein expression versus WT related to figure 5A; Error bars show standard deviation; statistical analysis was performed using multiple t-test (n = 3 mice/genotype). **C.** ChIP analysis for AID occupancy in Sμ and Sγ regions of primary B cells in response to LPS/IL-4/α-RP105 stimulation. Relative enrichment was calculated as ChIP/input. Error bars show standard deviation (n = 3 mice/genotype); statistical analysis versus *Aicda*$^{-/-}$ control was performed using the students t-test, * denotes p-value < 0.05 compared to *Aicda*$^{-/-}$. **D.** ChIP analysis for Pol ll (Ser5) occupancy in Sμ and Sγ regions of primary B cells in response to LPS/IL-4/α-RP105 stimulation. Relative enrichment was calculated as fold change relative to WT set to 1; error bars show standard deviation (n = 5 mice/genotype).

Figure 6. Model for SETX and RNase H2 in promoting efficient CSR. When B cells are stimulated to undergo class switching, PolII-mediated transcription opens duplex DNA at recombining S regions. R loops formed during transcription promote AID binding to ssDNA on the non-template strand first. SETX and RNase H2 then cooperate to remove switch region R loops, exposing ssDNA on the non-template strand for AID to bind. Extensive AID activity and uracil removal on both strands results in the formation of DSBs with limited ssDNA overhangs at break ends ("blunted" ends) which are predominantly repaired by cNHEJ. **B.** When SETX and RNase H2B are absent, R loops forming at S region are not efficiently removed. This persistent R loop/RNA:DNA hybrid may affect CSR in two ways. One possible mechanism for increased error-prone EJ is that persistent R loops reduce the extent of ssDNA available for AID binding specifically on the template

strand, increasing ssDNA tail length at DSB ends. Alternatively, persistent R loops may alter DNA repair protein recruitment to DSB ends. Both possibilities reduce cNHEJ efficiency, but do not affect overall CSR levels as the majority of breaks with long ssDNA tails are repaired by error-prone EJ. However a subset of breaks are not repaired, leading to persistent DSBs that manifest as chromosome breaks and translocations in mitotic spreads.

Supplementary figure 1. DNA:RNA hybrid formation at the *Actb* locus.

A. Representative UCSC genome browser screenshot of DRIP-Seq signal in WT, *Setx*$^{-/-}$, *Rnaseh2b*$^{f/f}$ and *Setx*$^{-/-}$ *Rnaseh2b*$^{f/f}$ cells spanning 10 kb of the *Actb* locus (n=2 mice/genotype). Locations of primers used in DRIP-qPCR shown in (**B**) are marked with black (gene body) and pink (3'UTR) triangles. **B.** DRIP-qPCR along *Actb* locus in mouse primary B cells. Error bars show the SEM from three independent experiments. Statistical analyses were performed using one-way ANOVA, n = 3 mice/genotype.

Supplementary Figure 2. RNP incorporation in cells lacking SETX and RNase H2.

A. Representative image of alkaline gel of genomic DNA (n=3 independent mice/genotype). **B.** Densitometry trace of representative alkaline gel shown in (**A**) with ImageJ software. **C.** Frequency of DNA damage in WT, *Setx*$^{-/-}$, *Rnaseh2b*$^{f/f}$ and *Setx*$^{-/-}$*Rnaseh2b*$^{f/f}$ cells after exposure to 5 nM CPT for 20 hours. **D.** Frequency of DNA damage at IgH in CPT-treated cells. All cells were harvested 72 hours post-stimulation to IgG1 with LPS/IL-4/α-RP105. Statistical significance versus WT was determined by one-way ANOVA (n = 3 independent mice/genotype).

Supplementary Figure 3. AID activity is required for persistent IgH breaks in *Setx*$^{-/-}$*Rnaseh2b*$^{f/f}$ B cells. A. AID protein levels in WT B cells 72 hours post-stimulation to indicated isotypes (IgG1, LPS/IL-4/α-RP105; IgG3 with LPS/α-RP105; and α-RP105 alone). Actin served as a loading control. **B.** Quantification of AID protein expression relative to Actin for three independent experiments, with AID expression in resting cells set as 1.

Error bars show standard deviation. **C.** Percent of cells undergoing CSR to IgG1 in B cells in response to α-CD180 stimulation. Error bars show standard deviation; statistical significance between each genotype was determined by one-way ANOVA(n = 3 mice/genotype). **D.** Frequency of total spontaneous DNA damage under Anti-CD180 treatment in vitro. Error bars show the SEM; statistical significance versus WT was determined by one-way ANOVA (n = 3 mice/genotype). **E.** Frequency of total spontaneous DNA damage 72 hours post-stimulation with LPS/IL-4/α-RP105. Error bars show the SD; statistical analysis was performed using one-way ANOVA (n = 2 mice/genotype). **F.** Frequency of spontaneous IgH damage Error bars show the SD; statistical analysis was performed using one-way ANOVA (n = 2 mice/genotype).

Supplementary Figure 4. *Aicda* mRNA levels in WT and mutant mice.

A. AID mRNA quantitation by RT-qPCR in resting cells, LPS/α-RP105/IL4, LPS/α-RP105, and α-RP105-only stimulated cells. Error bars show the SEM from three independent experiments.

Supplementary figure 5. B cell proliferation and cell cycle in response to stimulation.

A. Flow cytometry analysis of cell proliferation with CFSE staining. CFSE-labeled primary B cells were stimulated with LPS/IL-4/α-RP105 and cell division was measured by CFSE dye dilution at 72 hours post-stimulation. **B.** Representative flow cytometry analyses of IgG1 with CFSE staining in spleen primary B cells in response to LPS/IL-4/α-RP105. **C.** The percentage of cells in each cell cycle. Error bars show the SEM, statistical analyses were performed using one-way ANOVA (n = 3 mice per genotype). **D.** Representative cell cycle profiles for WT, *Setx*$^{-/-}$, *Rnaseh2b*$^{f/f}$ and *Setx*$^{-/-}$*Rnaseh2b*$^{f/f}$ cells stimulated with LPS/IL-4/α-RP105.

References

Aguilera A, Garcia-Muse T (2012) R loops: from transcription byproducts to threats to genome stability. *Mol Cell* 46: 115-124
Alt FW, Zhang Y, Meng FL, Guo C, Schwer B (2013) Mechanisms of programmed DNA lesions and genomic instability in the immune system. *Cell* 152: 417-429
Bardwell PD, Woo CJ, Wei K, Li Z, Martin A, Sack SZ, Parris T, Edelmann W, Scharff MD (2004) Altered somatic hypermutation and reduced class-switch recombination in exonuclease 1-mutant mice. *Nature immunology* 5: 224-229
Barlow JH, Faryabi RB, Callen E, Wong N, Malhowski A, Chen HT, Gutierrez-Cruz G, Sun HW, McKinnon P, Wright G *et al* (2013) Identification of early replicating fragile sites that contribute to genome instability. *Cell* 152: 620-632
Basu U, Meng FL, Keim C, Grinstein V, Pefanis E, Eccleston J, Zhang T, Myers D, Wasserman CR, Wesemann DR *et al* (2011) The RNA exosome targets the AID cytidine deaminase to both strands of transcribed duplex DNA substrates. *Cell* 144: 353-363
Becherel OJ, Yeo AJ, Stellati A, Heng EY, Luff J, Suraweera AM, Woods R, Fleming J, Carrie D, McKinney K *et al* (2013) Senataxin plays an essential role with DNA damage response proteins in meiotic recombination and gene silencing. *PLoS Genet* 9: e1003435
Bennardo N, Cheng A, Huang N, Stark JM (2008) Alternative-NHEJ Is a Mechanistically Distinct Pathway of Mammalian Chromosome Break Repair. *Plos Genetics* 4
Boboila C, Yan C, Wesemann DR, Jankovic M, Wang JH, Manis J, Nussenzweig A, Nussenzweig M, Alt FW (2010) Alternative end-joining catalyzes class switch recombination in the absence of both Ku70 and DNA ligase 4. *J Exp Med* 207: 417-427
Callen E, Jankovic M, Difilippantonio S, Daniel JA, Chen HT, Celeste A, Pellegrini M, McBride K, Wangsa D, Bredemeyer AL *et al* (2007) ATM prevents the persistence and propagation of chromosome breaks in lymphocytes. *Cell* 130: 63-75
Casellas R, Nussenzweig A, Wuerffel R, Pelanda R, Reichlin A, Suh H, Qin XF, Besmer E, Kenter A, Rajewsky K *et al* (1998) Ku80 is required for immunoglobulin isotype switching. *EMBO J* 17: 2404-2411
Chang HH, Watanabe G, Gerodimos CA, Ochi T, Blundell TL, Jackson SP, Lieber MR (2016) Different DNA End Configurations Dictate Which NHEJ Components Are Most Important for Joining Efficiency. *J Biol Chem* 291: 24377-24389
Chang HHY, Pannunzio NR, Adachi N, Lieber MR (2017) Non-homologous DNA end joining and alternative pathways to double-strand break repair. *Nat Rev Mol Cell Biol* 18: 495-506
Chaudhuri J, Khuong C, Alt FW (2004) Replication protein A interacts with AID to promote deamination of somatic hypermutation targets. *Nature* 430: 992-998
Chaudhuri J, Tian M, Khuong C, Chua K, Pinaud E, Alt FW (2003) Transcription-targeted DNA deamination by the AID antibody diversification enzyme. *Nature* 422: 726-730
Chon H, Sparks JL, Rychlik M, Nowotny M, Burgers PM, Crouch RJ, Cerritelli SM (2013) RNase H2 roles in genome integrity revealed by unlinking its activities. *Nucleic Acids Res* 41: 3130-3143
Cohen S, Puget N, Lin YL, Clouaire T, Aguirrebengoa M, Rocher V, Pasero P, Canitrot Y, Legube G (2018) Senataxin resolves RNA:DNA hybrids forming at DNA double-strand breaks to prevent translocations. *Nat Commun* 9: 533
Costantino L, Koshland D (2018) Genome-wide Map of R-Loop-Induced Damage Reveals How a Subset of R-Loops Contributes to Genomic Instability. *Mol Cell* 71: 487-497 e483
Crossley MP, Bocek M, Cimprich KA (2019) R-Loops as Cellular Regulators and Genomic Threats. *Mol Cell* 73: 398-411
Daniels GA, Lieber MR (1995) RNA:DNA complex formation upon transcription of immunoglobulin switch regions: implications for the mechanism and regulation of class switch recombination. *Nucleic Acids Res* 23: 5006-5011

Du L, van der Burg M, Popov SW, Kotnis A, van Dongen JJ, Gennery AR, Pan-Hammarstrom Q (2008) Involvement of Artemis in nonhomologous end-joining during immunoglobulin class switch recombination. *J Exp Med* 205: 3031-3040
Franco S, Murphy MM, Li G, Borjeson T, Boboila C, Alt FW (2008) DNA-PKcs and Artemis function in the end-joining phase of immunoglobulin heavy chain class switch recombination. *J Exp Med* 205: 557-564
Ginno PA, Lott PL, Christensen HC, Korf I, Chedin F (2012) R-Loop Formation Is a Distinctive Characteristic of Unmethylated Human CpG Island Promoters. *Molecular Cell* 45: 814-825
Grigera F, Wuerffel R, Kenter AL (2017) MBD4 Facilitates Immunoglobulin Class Switch Recombination. *Mol Cell Biol* 37
Gu Y, Seidl KJ, Rathbun GA, Zhu C, Manis JP, van der Stoep N, Davidson L, Cheng HL, Sekiguchi JM, Frank K *et al* (1997) Growth retardation and leaky SCID phenotype of Ku70-deficient mice. *Immunity* 7: 653-665
Hein K, Lorenz MG, Siebenkotten G, Petry K, Christine R, Radbruch A (1998) Processing of switch transcripts is required for targeting of antibody class switch recombination. *J Exp Med* 188: 2369-2374
Hiller B, Achleitner M, Glage S, Naumann R, Behrendt R, Roers A (2012) Mammalian RNase H2 removes ribonucleotides from DNA to maintain genome integrity. *J Exp Med* 209: 1419-1426
Hodgkin PD, Lee JH, Lyons AB (1996) B cell differentiation and isotype switching is related to division cycle number. *J Exp Med* 184: 277-281
Hodroj D, Recolin B, Serhal K, Martinez S, Tsanov N, Abou Merhi R, Maiorano D (2017) An ATR-dependent function for the Ddx19 RNA helicase in nuclear R-loop metabolism. *EMBO J* 36: 1182-1198
Huang FT, Yu K, Balter BB, Selsing E, Oruc Z, Khamlichi AA, Hsieh CL, Lieber MR (2007) Sequence dependence of chromosomal R-loops at the immunoglobulin heavy-chain Smu class switch region. *Mol Cell Biol* 27: 5921-5932
Huang SN, Williams JS, Arana ME, Kunkel TA, Pommier Y (2017) Topoisomerase I-mediated cleavage at unrepaired ribonucleotides generates DNA double-strand breaks. *EMBO J* 36: 361-373
Kazadi D, Lim J, Rothschild G, Grinstein V, Laffleur B, Becherel O, Lavin MJ, Basu U (2020) Effects of senataxin and RNA exosome on B-cell chromosomal integrity. *Heliyon* 6: e03442
Kuznetsov VA, Bondarenko V, Wongsurawat T, Yenamandra SP, Jenjaroenpun P (2018) Toward predictive R-loop computational biology: genome-scale prediction of R-loops reveals their association with complex promoter structures, G-quadruplexes and transcriptionally active enhancers (vol 46, pg 7566, 2018). *Nucleic Acids Research* 46: 8023-8023
Lee-Theilen M, Matthews AJ, Kelly D, Zheng S, Chaudhuri J (2011) CtIP promotes microhomology-mediated alternative end joining during class-switch recombination. *Nat Struct Mol Biol* 18: 75-79
Li L, Halaby MJ, Hakem A, Cardoso R, El Ghamrasni S, Harding S, Chan N, Bristow R, Sanchez O, Durocher D *et al* (2010) Rnf8 deficiency impairs class switch recombination, spermatogenesis, and genomic integrity and predisposes for cancer. *J Exp Med* 207: 983-997
Lumsden JM, McCarty T, Petiniot LK, Shen R, Barlow C, Wynn TA, Morse HC, Gearhart PJ, Wynshaw-Boris A, Max EE *et al* (2004) Immunoglobulin class switch recombination is impaired in Atm-deficient mice. *J Exp Med* 200: 1111-1121
Lyons AB, Parish CR (1994) Determination of lymphocyte division by flow cytometry. *J Immunol Methods* 171: 131-137
Manis JP, Dudley D, Kaylor L, Alt FW (2002) IgH class switch recombination to IgG1 in DNA-PKcs-deficient B cells. *Immunity* 16: 607-617
Marchalot A, Ashi MO, Lambert JM, Carrion C, Lecardeur S, Srour N, Delpy L, Le Pennec S (2020) Uncoupling Splicing From Transcription Using Antisense Oligonucleotides Reveals a Dual Role for I Exon Donor Splice Sites in Antibody Class Switching. *Front Immunol* 11: 780
Marnef A, Legube G (2021) R-loops as Janus-faced modulators of DNA repair. *Nature cell biology* 23: 305-313
Maul RW, Chon H, Sakhuja K, Cerritelli SM, Gugliotti LA, Gearhart PJ, Crouch RJ (2017) R-Loop Depletion by Over-expressed RNase H1 in Mouse B Cells Increases Activation-Induced Deaminase Access to the Transcribed Strand without Altering Frequency of Isotype Switching. *Journal of molecular biology* 429: 3255-3263

Mcdonell MW, Simon MN, Studier FW (1977) Analysis of Restriction Fragments of T7 DNA and Determination of Molecular-Weights by Electrophoresis in Neutral and Alkaline Gels. *J Mol Biol* 110: 119-146
Muramatsu M, Kinoshita K, Fagarasan S, Yamada S, Shinkai Y, Honjo T (2000) Class switch recombination and hypermutation require activation-induced cytidine deaminase (AID), a potential RNA editing enzyme. *Cell* 102: 553-563
Nick McElhinny SA, Kumar D, Clark AB, Watt DL, Watts BE, Lundstrom EB, Johansson E, Chabes A, Kunkel TA (2010) Genome instability due to ribonucleotide incorporation into DNA. *Nature chemical biology* 6: 774-781
Nussenzweig A, Nussenzweig MC (2007) A backup DNA repair pathway moves to the forefront. *Cell* 131: 223-225
Parsa JY, Ramachandran S, Zaheen A, Nepal RM, Kapelnikov A, Belcheva A, Berru M, Ronai D, Martin A (2012) Negative supercoiling creates single-stranded patches of DNA that are substrates for AID-mediated mutagenesis. *PLoS Genet* 8: e1002518
Pavri R, Gazumyan A, Jankovic M, Di Virgilio M, Klein I, Ansarah-Sobrinho C, Resch W, Yamane A, Reina San-Martin B, Barreto V *et al* (2010) Activation-induced cytidine deaminase targets DNA at sites of RNA polymerase II stalling by interaction with Spt5. *Cell* 143: 122-133
Pham P, Bransteitter R, Petruska J, Goodman MF (2003) Processive AID-catalysed cytosine deamination on single-stranded DNA simulates somatic hypermutation. *Nature* 424: 103-107
Prado F, Aguilera A (2005) Impairment of replication fork progression mediates RNA polII transcription-associated recombination. *EMBO J* 24: 1267-1276
Qiao Q, Wang L, Meng FL, Hwang JK, Alt FW, Wu H (2017) AID Recognizes Structured DNA for Class Switch Recombination. *Mol Cell* 67: 361-373 e364
Ramiro AR, Jankovic M, Eisenreich T, Difilippantonio S, Chen-Kiang S, Muramatsu M, Honjo T, Nussenzweig A, Nussenzweig MC (2004) AID is required for c-myc/IgH chromosome translocations in vivo. *Cell* 118: 431-438
Ramiro AR, Stavropoulos P, Jankovic M, Nussenzweig MC (2003a) Transcription enhances AID-mediated cytidine deamination by exposing single-stranded DNA on the nontemplate strand. *Nat Immunol* 4: 452-456
Ramiro AR, Stavropoulos P, Jankovic M, Nussenzweig MC (2003b) Transcription enhances AID-mediated cytidine deamination by exposing single-stranded DNA on the nontemplate strand. *Nature immunology* 4: 452-456
Reaban ME, Griffin JA (1990) Induction of RNA-stabilized DNA conformers by transcription of an immunoglobulin switch region. *Nature* 348: 342-344
Reijns MA, Rabe B, Rigby RE, Mill P, Astell KR, Lettice LA, Boyle S, Leitch A, Keighren M, Kilanowski F *et al* (2012) Enzymatic removal of ribonucleotides from DNA is essential for mammalian genome integrity and development. *Cell* 149: 1008-1022
Reina-San-Martin B, Chen HT, Nussenzweig A, Nussenzweig MC (2004) ATM is required for efficient recombination between immunoglobulin switch regions. *J Exp Med* 200: 1103-1110
Revy P, Muto T, Levy Y, Geissmann F, Plebani A, Sanal O, Catalan N, Forveille M, Dufourcq-Labelouse R, Gennery A *et al* (2000) Activation-induced cytidine deaminase (AID) deficiency causes the autosomal recessive form of the Hyper-IgM syndrome (HIGM2). *Cell* 102: 565-575
Ribeiro de Almeida C, Dhir S, Dhir A, Moghaddam AE, Sattentau Q, Meinhart A, Proudfoot NJ (2018) RNA Helicase DDX1 Converts RNA G-Quadruplex Structures into R-Loops to Promote IgH Class Switch Recombination. *Mol Cell* 70: 650-662 e658
Richard P, Feng S, Tsai YL, Li W, Rinchetti P, Muhith U, Irizarry-Cole J, Stolz K, Sanz LA, Hartono S *et al* (2020) SETX (senataxin), the helicase mutated in AOA2 and ALS4, functions in autophagy regulation. *Autophagy*: 1-18
Rickert RC, Roes J, Rajewsky K (1997) B lymphocyte-specific, Cre-mediated mutagenesis in mice. *Nucleic Acids Res* 25: 1317-1318
Rivera-Munoz P, Soulas-Sprauel P, Le Guyader G, Abramowski V, Bruneau S, Fischer A, Paques F, de Villartay JP (2009) Reduced immunoglobulin class switch recombination in the absence of Artemis. *Blood* 114: 3601-3609

Robbiani DF, Bothmer A, Callen E, Reina-San-Martin B, Dorsett Y, Difilippantonio S, Bolland DJ, Chen HT, Corcoran AE, Nussenzweig A *et al* (2008) AID is required for the chromosomal breaks in c-myc that lead to c-myc/IgH translocations. *Cell* 135: 1028-1038
Robbiani DF, Bunting S, Feldhahn N, Bothmer A, Camps J, Deroubaix S, McBride KM, Klein IA, Stone G, Eisenreich TR *et al* (2009) AID produces DNA double-strand breaks in non-Ig genes and mature B cell lymphomas with reciprocal chromosome translocations. *Mol Cell* 36: 631-641
Roberts SA, Strande N, Burkhalter MD, Strom C, Havener JM, Hasty P, Ramsden DA (2010) Ku is a 5'-dRP/AP lyase that excises nucleotide damage near broken ends. *Nature* 464: 1214-1217
Roy D, Yu K, Lieber MR (2008) Mechanism of R-loop formation at immunoglobulin class switch sequences. *Mol Cell Biol* 28: 50-60
Santos MA, Huen MS, Jankovic M, Chen HT, Lopez-Contreras AJ, Klein IA, Wong N, Barbancho JL, Fernandez-Capetillo O, Nussenzweig MC *et al* (2010) Class switching and meiotic defects in mice lacking the E3 ubiquitin ligase RNF8. *J Exp Med* 207: 973-981
Sanz LA, Hartono SR, Lim YW, Steyaert S, Rajpurkar A, Ginno PA, Xu X, Chedin F (2016) Prevalent, Dynamic, and Conserved R-Loop Structures Associate with Specific Epigenomic Signatures in Mammals. *Mol Cell* 63: 167-178
Schrader CE, Vardo J, Stavnezer J (2002) Role for mismatch repair proteins Msh2, Mlh1, and Pms2 in immunoglobulin class switching shown by sequence analysis of recombination junctions. *J Exp Med* 195: 367-373
Serrano-Benitez A, Cortes-Ledesma F, Ruiz JF (2019) "An End to a Means": How DNA-End Structure Shapes the Double-Strand Break Repair Process. *Front Mol Biosci* 6: 153
So CC, Martin A (2019) DSB structure impacts DNA recombination leading to class switching and chromosomal translocations in human B cells. *PLoS Genet* 15: e1008101
Sohail A, Klapacz J, Samaranayake M, Ullah A, Bhagwat AS (2003) Human activation-induced cytidine deaminase causes transcription-dependent, strand-biased C to U deaminations. *Nucleic Acids Research* 31: 2990-2994
Sollier J, Stork CT, Garcia-Rubio ML, Paulsen RD, Aguilera A, Cimprich KA (2014) Transcription-Coupled Nucleotide Excision Repair Factors Promote R-Loop-Induced Genome Instability. *Molecular Cell* 56: 777-785
Song CL, Hotz-Wagenblatt A, Voit R, Grummt I (2017) SIRT7 and the DEAD-box helicase DDX21 cooperate to resolve genomic R loops and safeguard genome stability. *Genes & Development* 31: 1370-1381
Soulas-Sprauel P, Le Guyader G, Rivera-Munoz P, Abramowski V, Olivier-Martin C, Goujet-Zalc C, Charneau P, de Villartay JP (2007) Role for DNA repair factor XRCC4 in immunoglobulin class switch recombination. *J Exp Med* 204: 1717-1727
Stanlie A, Begum NA, Akiyama H, Honjo T (2012) The DSIF subunits Spt4 and Spt5 have distinct roles at various phases of immunoglobulin class switch recombination. *PLoS Genet* 8: e1002675
Stavnezer J, Schrader CE (2014) IgH chain class switch recombination: mechanism and regulation. *J Immunol* 193: 5370-5378
Stolz R, Sulthana S, Hartono SR, Malig M, Benham CJ, Chedin F (2019) Interplay between DNA sequence and negative superhelicity drives R-loop structures. *P Natl Acad Sci USA* 116: 6260-6269
Stork CT, Bocek M, Crossley MP, Sollier J, Sanz LA, Chedin F, Swigut T, Cimprich KA (2016) Co-transcriptional R-loops are the main cause of estrogen-induced DNA damage. *Elife* 5
Strande N, Roberts SA, Oh S, Hendrickson EA, Ramsden DA (2012) Specificity of the dRP/AP lyase of Ku promotes nonhomologous end joining (NHEJ) fidelity at damaged ends. *J Biol Chem* 287: 13686-13693
Symington LS (2016) Mechanism and regulation of DNA end resection in eukaryotes. *Crit Rev Biochem Mol Biol* 51: 195-212
Uchimura Y, Barton LF, Rada C, Neuberger MS (2011) REG-gamma associates with and modulates the abundance of nuclear activation-induced deaminase. *J Exp Med* 208: 2385-2391
Waisertreiger I, Popovich K, Block M, Anderson KR, Barlow JH (2020) Visualizing locus-specific sister chromatid exchange reveals differential patterns of replication stress-induced fragile site breakage. *Oncogene* 39: 1260-1272

Ward IM, Reina-San-Martin B, Olaru A, Minn K, Tamada K, Lau JS, Cascalho M, Chen L, Nussenzweig A, Livak F *et al* (2004) 53BP1 is required for class switch recombination. *J Cell Biol* 165: 459-464
Wiedemann EM, Peycheva M, Pavri R (2016) DNA Replication Origins in Immunoglobulin Switch Regions Regulate Class Switch Recombination in an R-Loop-Dependent Manner. *Cell reports* 17: 2927-2942
Williams JS, Kunkel TA (2014) Ribonucleotides in DNA: origins, repair and consequences. *DNA repair* 19: 27-37
Williams JS, Smith DJ, Marjavaara L, Lujan SA, Chabes A, Kunkel TA (2013) Topoisomerase 1-mediated removal of ribonucleotides from nascent leading-strand DNA. *Mol Cell* 49: 1010-1015
Yamane A, Resch W, Kuo N, Kuchen S, Li Z, Sun HW, Robbiani DF, McBride K, Nussenzweig MC, Casellas R (2011) Deep-sequencing identification of the genomic targets of the cytidine deaminase AID and its cofactor RPA in B lymphocytes. *Nature immunology* 12: 62-69
Yan CT, Boboila C, Souza EK, Franco S, Hickernell TR, Murphy M, Gumaste S, Geyer M, Zarrin AA, Manis JP *et al* (2007) IgH class switching and translocations use a robust non-classical end-joining pathway. *Nature* 449: 478-482
Yu K, Chedin F, Hsieh CL, Wilson TE, Lieber MR (2003) R-loops at immunoglobulin class switch regions in the chromosomes of stimulated B cells. *Nature immunology* 4: 442-451
Zhang ZZ, Pannunzio NR, Hsieh CL, Yu K, Lieber MR (2014) The role of G-density in switch region repeats for immunoglobulin class switch recombination. *Nucleic Acids Res* 42: 13186-13193
Zheng SM, Vuong BQ, Vaidyanathan B, Lin JY, Huang FT, Chaudhuri J (2015) Non-coding RNA Generated following Lariat Debranching Mediates Targeting of AID to DNA. *Cell* 161: 762-773

Figure 1

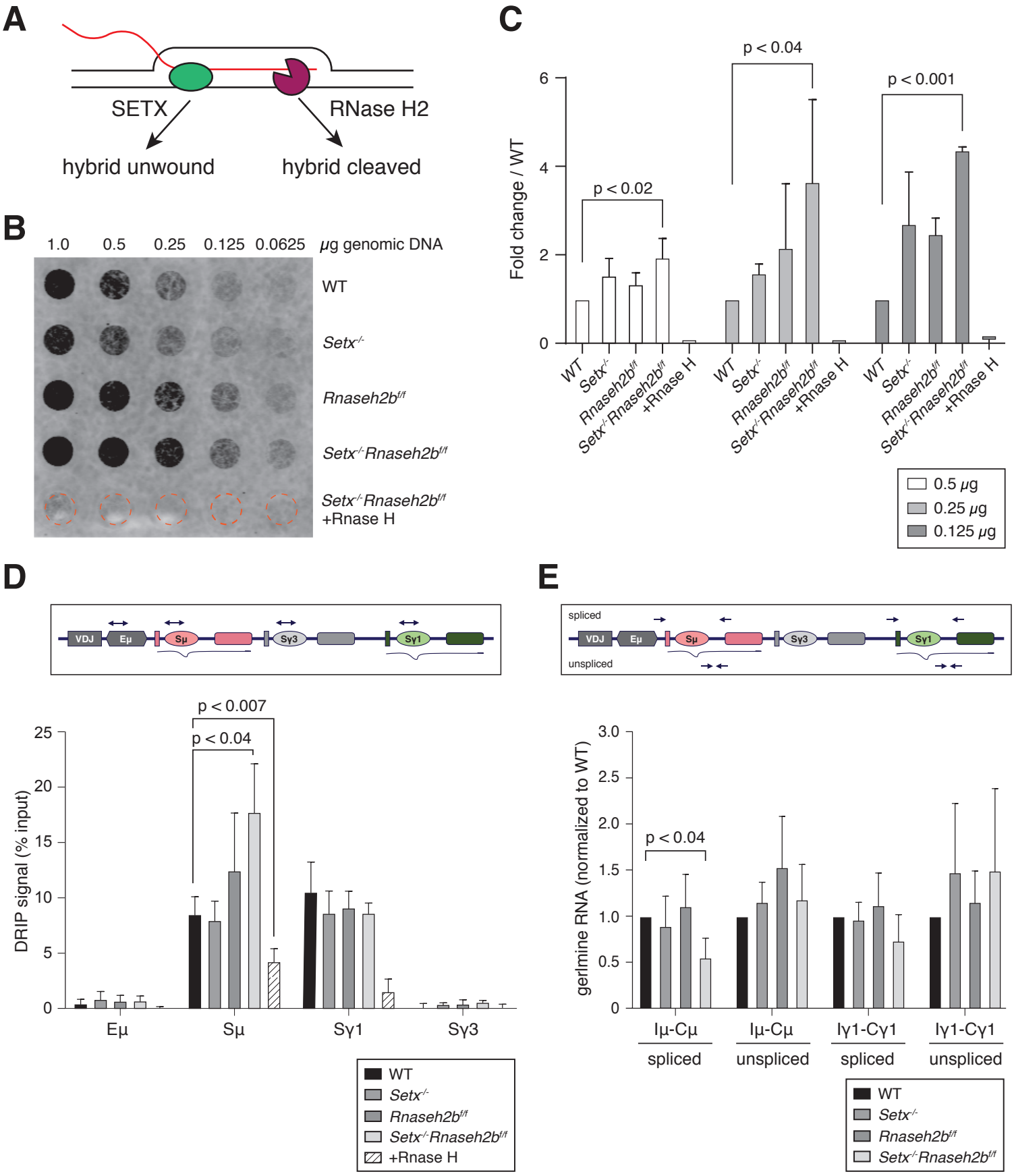
A
SETX
RNase H2
hybrid unwound
hybrid cleaved
B
1.0
0.5
0.25
0.125
0.0625
μg genomic DNA
WT
Setx-/-
Rnaseh2bf/f
Setx-/-Rnaseh2bf/f
Setx-/-Rnaseh2bf/f +Rnase H
C
Fold change / WT
p < 0.02
p < 0.04
p < 0.001
WT
Setx-/-
Rnaseh2bf/f
Setx-/-Rnaseh2bf/f
+Rnase H
0.5 μg
0.25 μg
0.125 μg
D
VDJ
Eμ
Sμ
Sγ3
Sγ1
DRIP signal (% input)
p < 0.007
p < 0.04
Eμ
Sμ
Sγ1
Sγ3
WT
Setx-/-
Rnaseh2bf/f
Setx-/-Rnaseh2bf/f
+Rnase H
E
spliced
unspliced
germline RNA (normalized to WT)
p < 0.04
Iμ-Cμ
Iγ1-Cγ1
spliced
unspliced
WT
Setx-/-
Rnaseh2bf/f
Setx-/-Rnaseh2bf/f

Figure 2

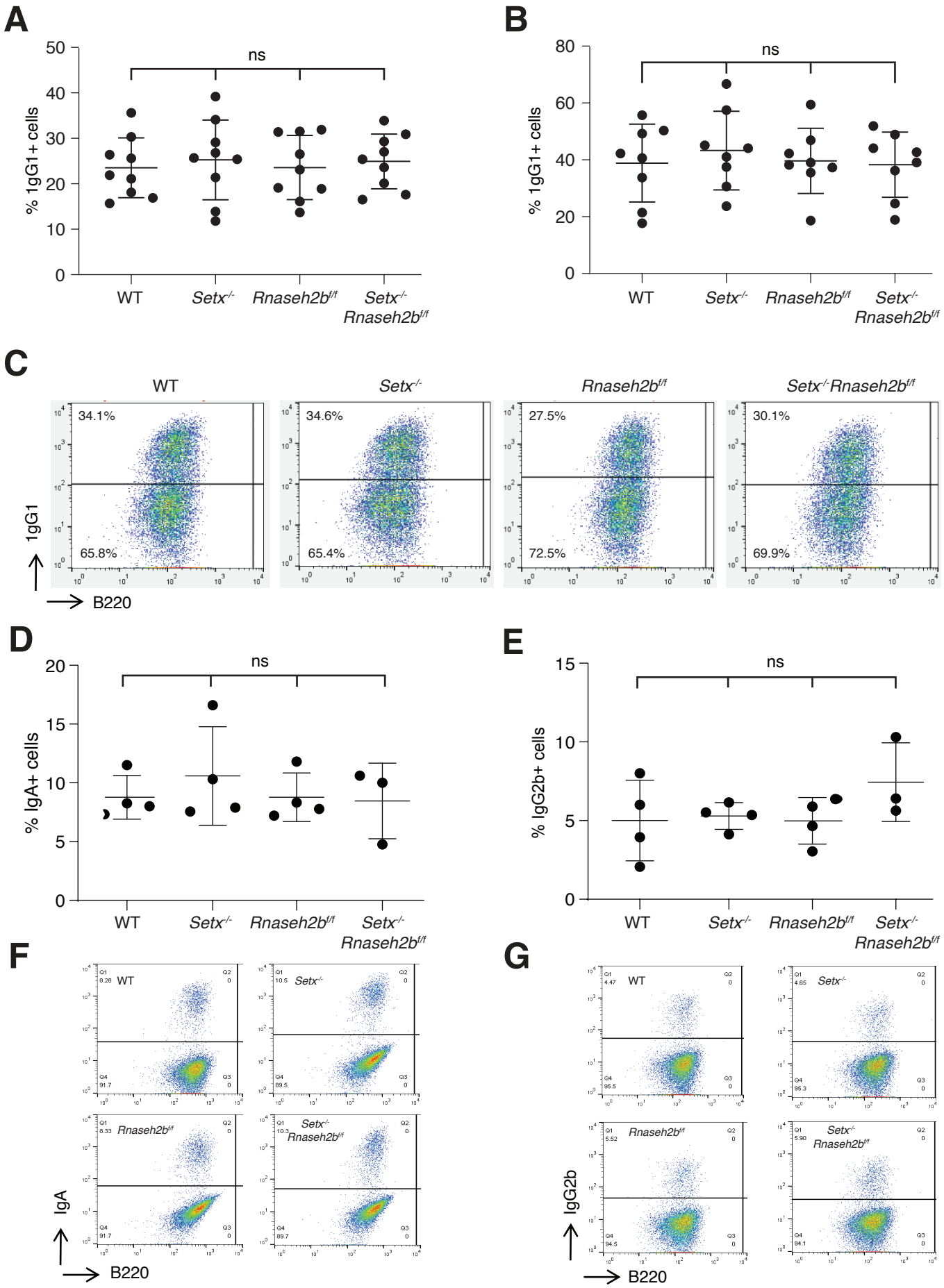
A
ns
% 1gG1+ cells
WT
Setx-/-
Rnaseh2bf/f
Setx-/- Rnaseh2bf/f
B
ns
% 1gG1+ cells
C
WT
Setx-/-
Rnaseh2bf/f
Setx-/-Rnaseh2bf/f
34.1%
65.8%
34.6%
65.4%
27.5%
72.5%
30.1%
69.9%
1gG1
B220
D
ns
% IgA+ cells
E
ns
% IgG2b+ cells
F
WT
Setx-/-
Rnaseh2bf/f
Setx-/- Rnaseh2bf/f
IgA
B220
G
WT
Setx-/-
Rnaseh2bf/f
Setx-/- Rnaseh2bf/f
IgG2b
B220

Figure 3

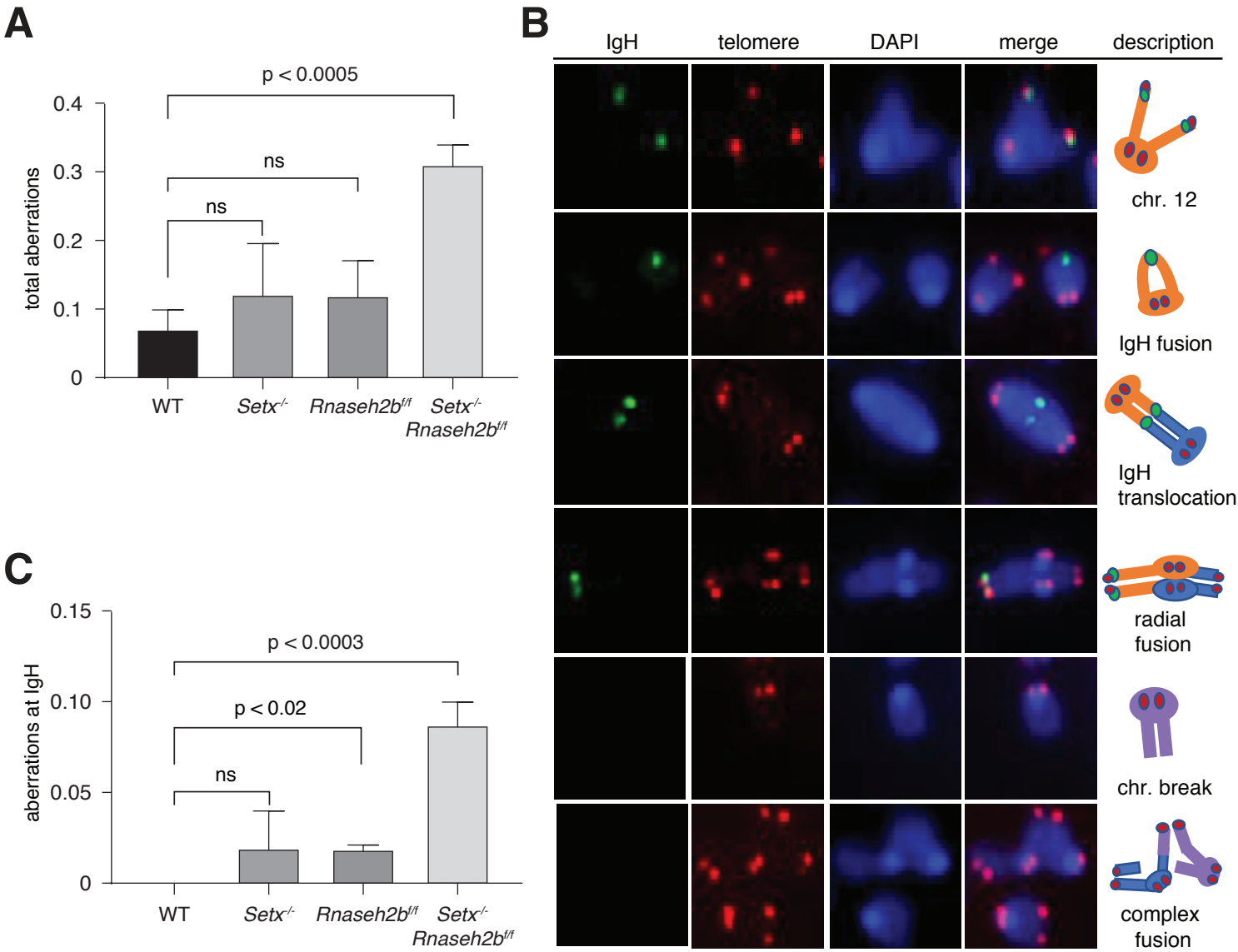
A
p < 0.0005
ns
ns
total aberrations
0.4
0.3
0.2
0.1
0
WT
Setx-/-
Rnaseh2bf/f
Setx-/- Rnaseh2bf/f
B
IgH
telomere
DAPI
merge
description
chr. 12
IgH fusion
IgH translocation
radial fusion
chr. break
complex fusion
C
p < 0.0003
p < 0.02
ns
aberrations at IgH
0.15
0.10
0.05
0
WT
Setx-/-
Rnaseh2bf/f
Setx-/- Rnaseh2bf/f

Figure 4

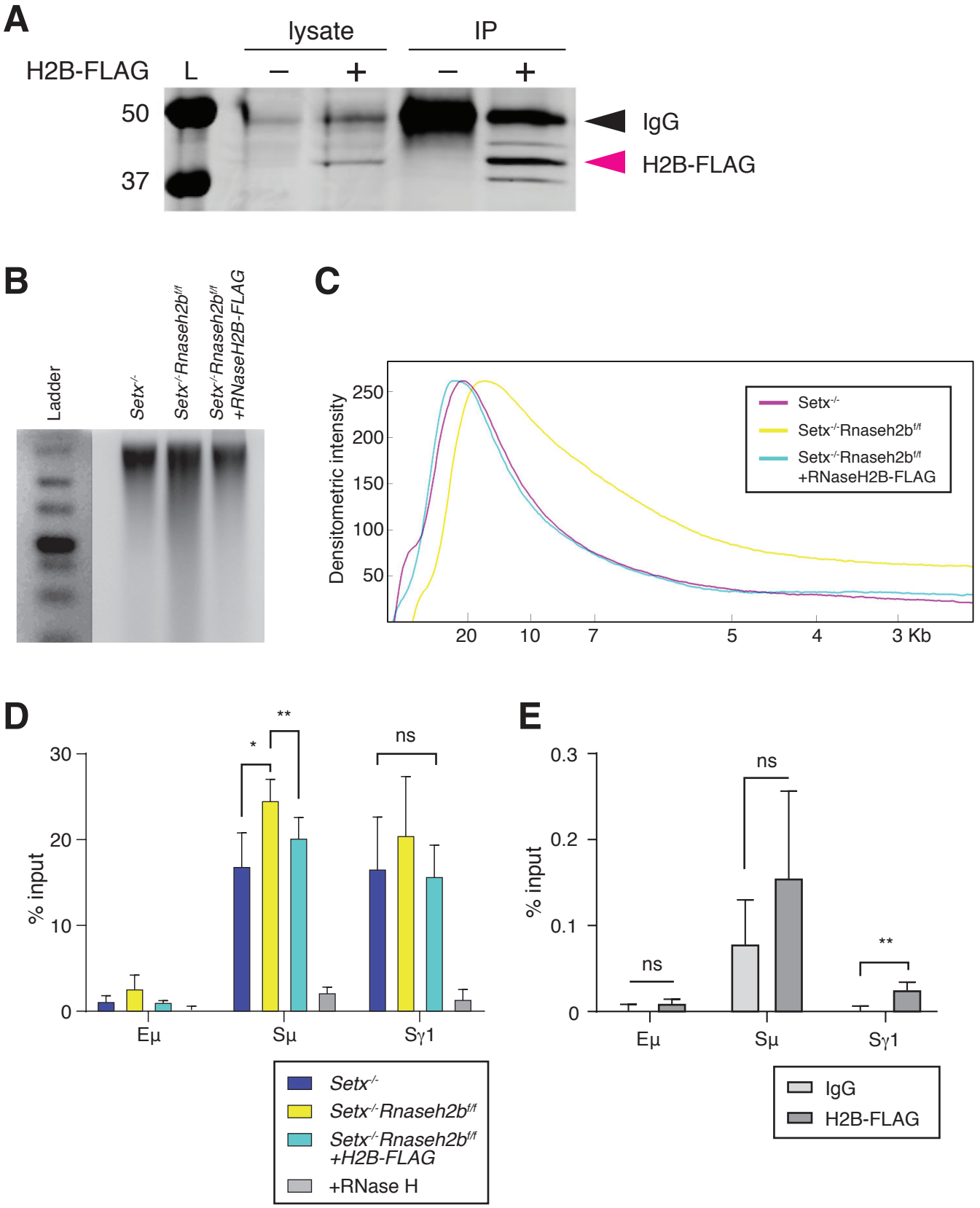
A
lysate
IP
H2B-FLAG
L
−
+
−
+
50
37
IgG
H2B-FLAG
B
Ladder
Setx-/-
Setx-/-Rnaseh2bf/f
Setx-/-Rnaseh2bf/f +RNaseH2B-FLAG
C
Densitometric intensity
250
200
150
100
50
20
10
7
5
4
3 Kb
Setx-/-
Setx-/-Rnaseh2bf/f
Setx-/-Rnaseh2bf/f +RNaseH2B-FLAG
D
% input
30
20
10
0
*
**
ns
Eμ
Sμ
Sγ1
Setx-/-
Setx-/-Rnaseh2bf/f
Setx-/-Rnaseh2bf/f +H2B-FLAG
+RNase H
E
% input
0.3
0.2
0.1
0
ns
ns
**
Eμ
Sμ
Sγ1
IgG
H2B-FLAG

Figure 5

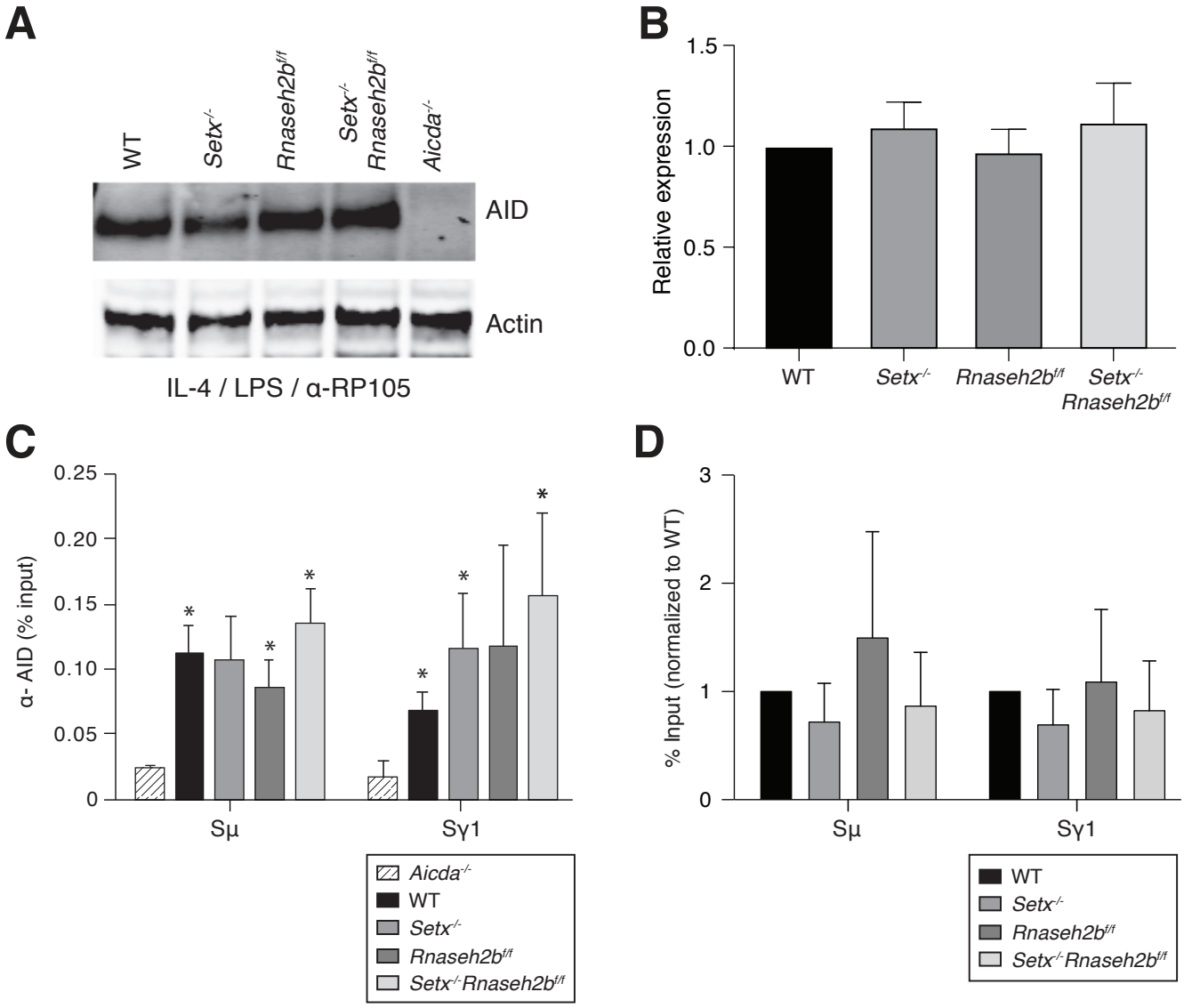
A
WT
Setx-/-
Rnaseh2bf/f
Setx-/- Rnaseh2bf/f
Aicda-/-
AID
Actin
IL-4 / LPS / α-RP105
B
Relative expression
1.5
1.0
0.5
0.0
WT
Setx-/-
Rnaseh2bf/f
Setx-/- Rnaseh2bf/f
C
α- AID (% input)
0.25
0.20
0.15
0.10
0.05
0
Sμ
Sγ1
Aicda-/-
WT
Setx-/-
Rnaseh2bf/f
Setx-/-Rnaseh2bf/f
D
% Input (normalized to WT)
3
2
1
0
Sμ
Sγ1
WT
Setx-/-
Rnaseh2bf/f
Setx-/-Rnaseh2bf/f

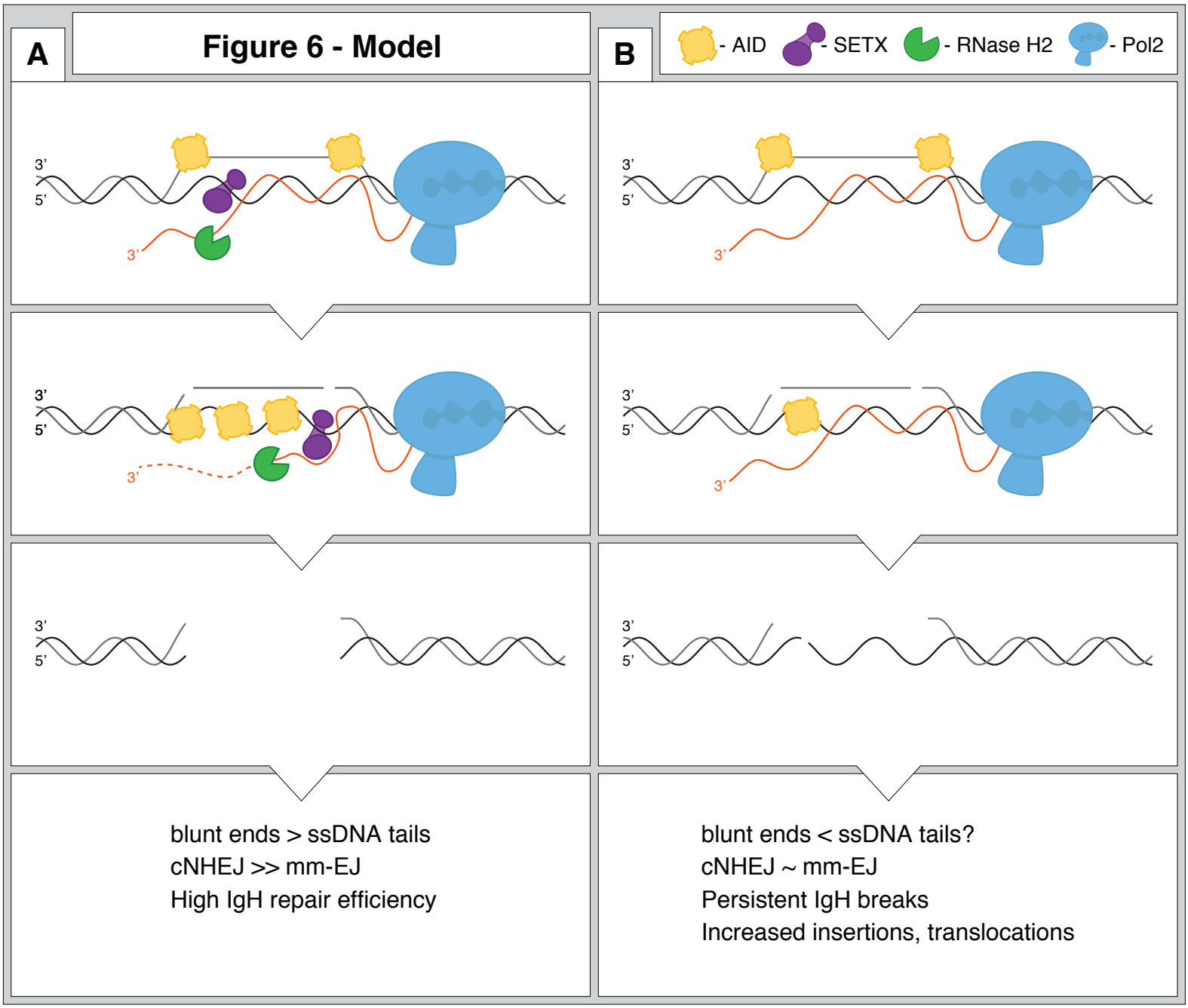
A
Figure 6 - Model
B
- AID
- SETX
- RNase H2
- Pol2
3'
5'
3'
blunt ends > ssDNA tails
cNHEJ >> mm-EJ
High IgH repair efficiency
blunt ends < ssDNA tails?
cNHEJ ~ mm-EJ
Persistent IgH breaks
Increased insertions, translocations

Supplementary Figure 1

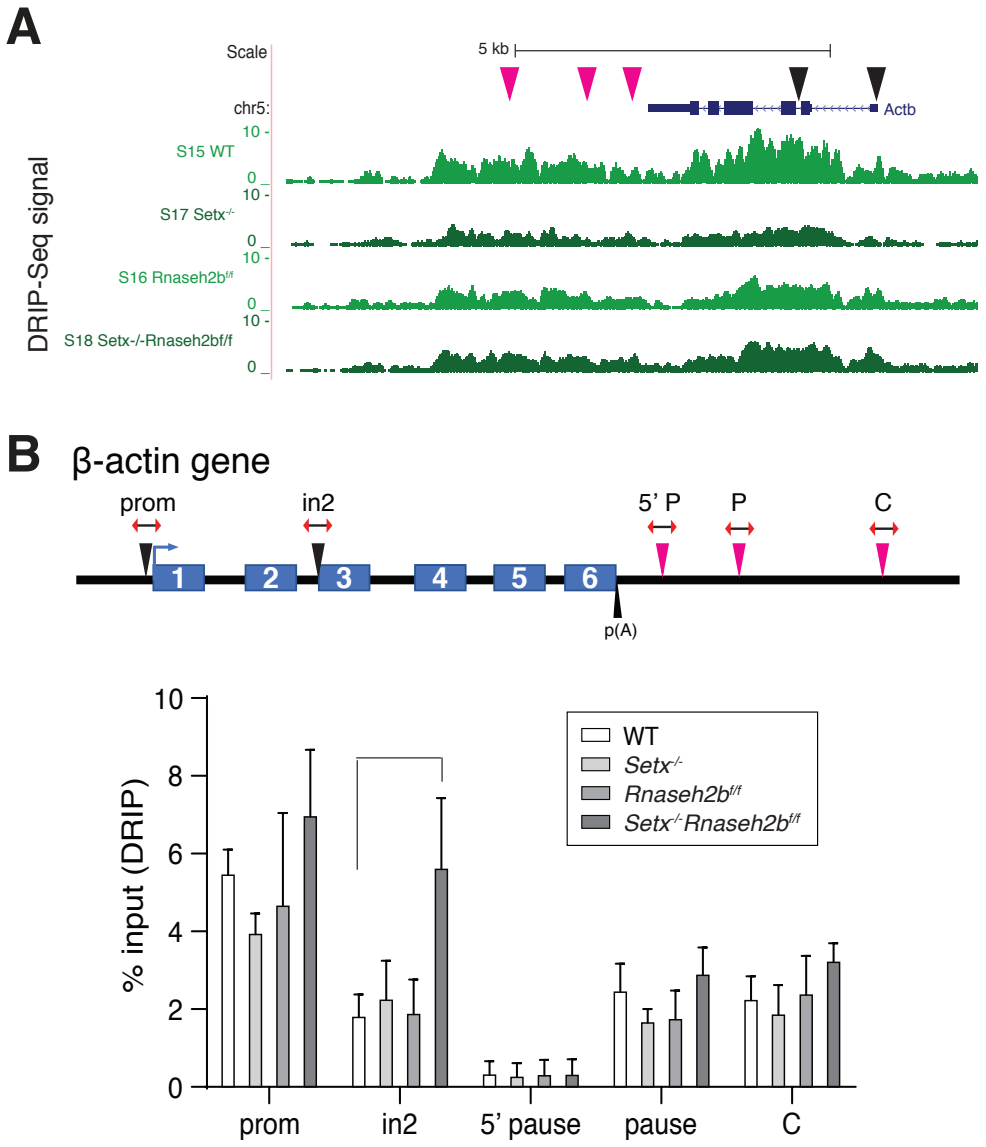

Supplementary Figure 2

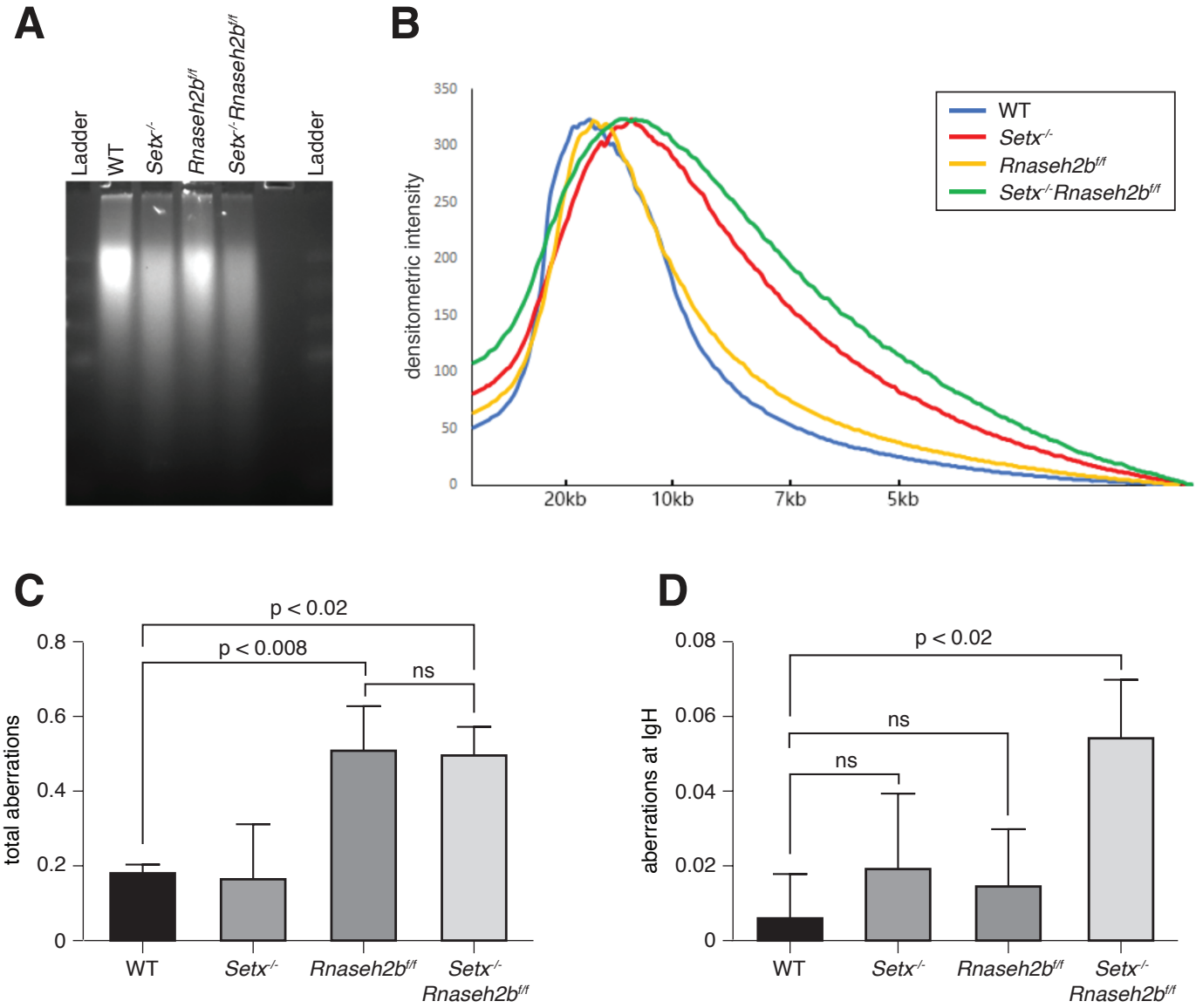

Supplementary Figure S3

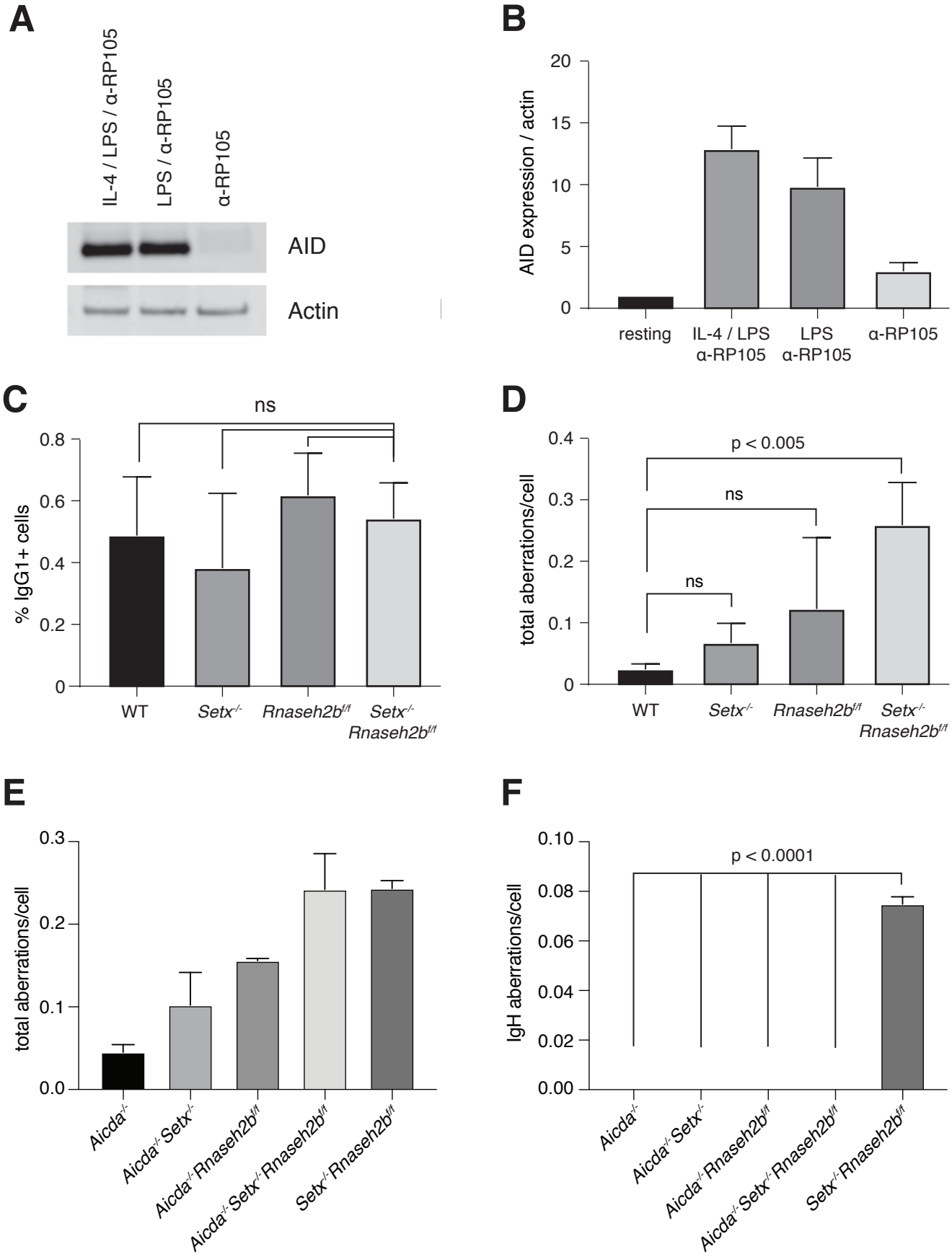

Supplementary figure 4

A

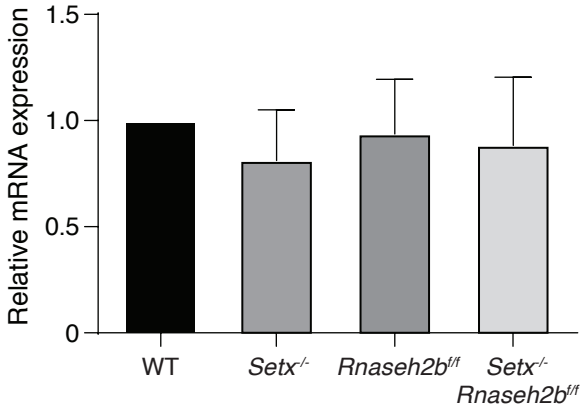

Supplementary Figure 5

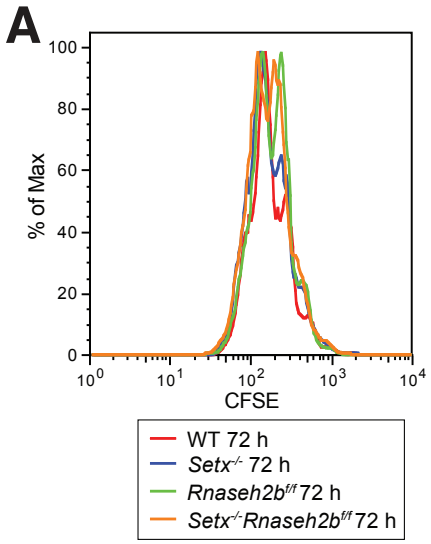

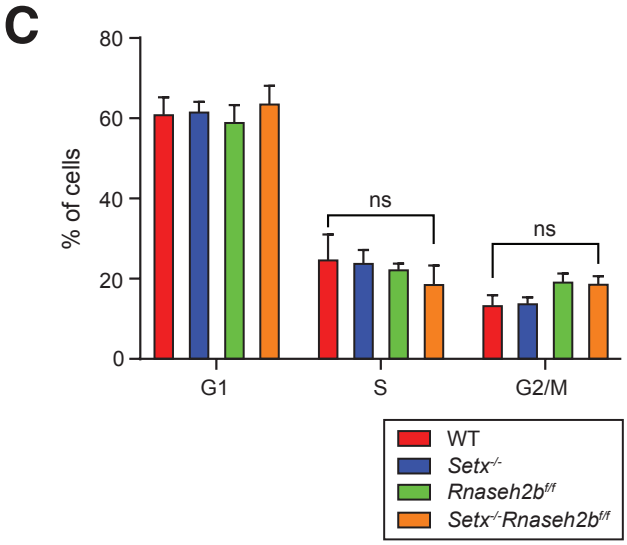

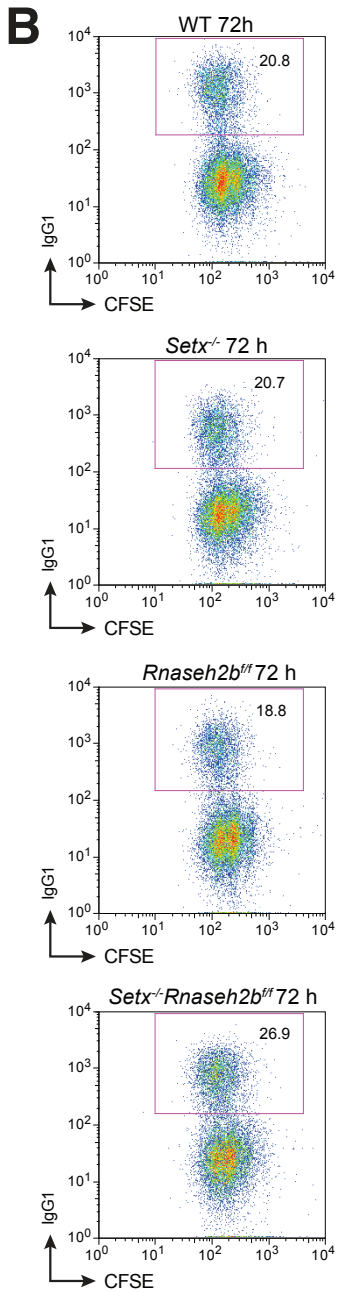

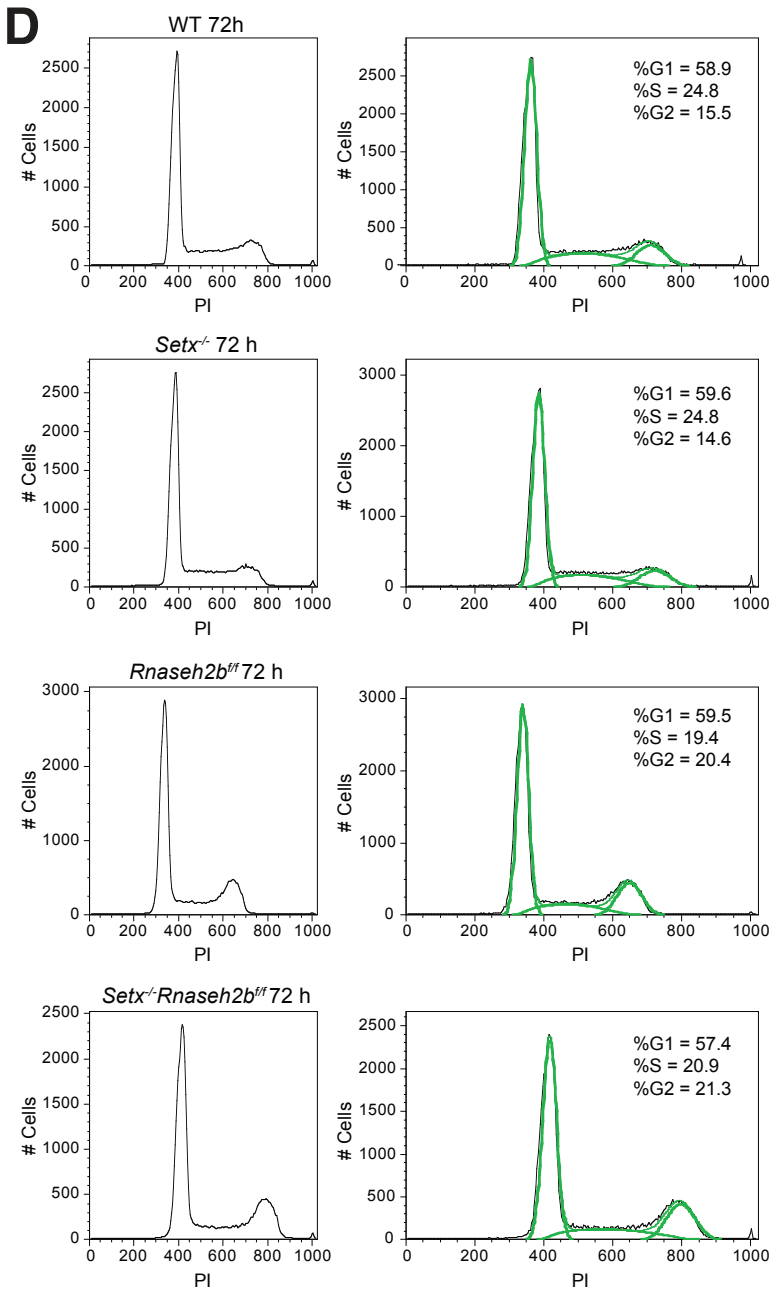

Supplementary Table 1: Summary of individual FISH results for experiments shown in Figure 3a, Figure 3c, and Supplementary figure 3d-f.

Experiment	Genotype	stimulation	total aberrations/cell	aberrations at IgH/cell	# cells analyzed
1	WT	RP105+LPS+IL-4	0.086207	0	58
	Setx-/-	RP105+LPS+IL-4	0.206896552	0.017241	58
	Rnaseh2bf/f	RP105+LPS+IL-4	0.0625	0.020833	48
	Setx-/-Rnaseh2bf/f	RP105+LPS+IL-4	0.326923	0.096154	52
2	WT	RP105+LPS+IL-4	0.087719	0	57
	Setx-/-	RP105+LPS+IL-4	0.075471698	0	53
	Rnaseh2bf/f	RP105+LPS+IL-4	0.134615385	0.019231	52
	Setx-/-Rnaseh2bf/f	RP105+LPS+IL-4	0.327273	0.072727	55
3	WT	RP105+LPS+IL-4	0.096153846	0	52
	Setx-/-	RP105+LPS+IL-4	0.06	0	50
	Rnaseh2bf/f	RP105+LPS+IL-4	0.096153846	0.019230769	52
	Setx-/-Rnaseh2bf/f	RP105+LPS+IL-4	0.245283019	0.075471698	53
4	WT	RP105	0.020408	0	49
	Setx-/-	RP105	0.096154	0	52
	Rnaseh2bf/f	RP105	0.022727	0	44
	Setx-/-Rnaseh2bf/f	RP105	0.333333	0	51
5	WT	RP105	0.034483	0	58
	Setx-/-	RP105	0.072464	0	69
	Rnaseh2bf/f	RP105	0.25	0	60
	Setx-/-Rnaseh2bf/f	RP105	0.246753	0	77
6	WT	RP105	0.017857	0	56
	Setx-/-	RP105	0.033333	0	60
	Rnaseh2bf/f	RP105	0.09434	0	53
	Setx-/-Rnaseh2bf/f	RP105	0.196078	0	51
7	AID-/-	RP105+LPS+IL-4	0.0517	0	58
	AID-/-Setx-/-	RP105+LPS+IL-4	0.13	0	55
	AID-/-Rnaseh2bf/f	RP105+LPS+IL-4	0.1578	0	57
	AID-/-Setx-/-Rnaseh2bf/f	RP105+LPS+IL-4	0.2727	0	55
	Setx-/-Rnaseh2bf/f	RP105+LPS+IL-4	0.2363	0.072727	55
8	AID-/-	RP105+LPS+IL-4	0.038461538	0	52
	AID-/-Setx-/-	RP105+LPS+IL-4	0.074074074	0	54
	AID-/-Rnaseh2bf/f	RP105+LPS+IL-4	0.153846154	0	52
	AID-/-Setx-/-Rnaseh2bf/f	RP105+LPS+IL-4	0.211538462	0	52
	Setx-/-Rnaseh2bf/f	RP105+LPS+IL-4	0.25	0.076923077	52

Supplementary table 2: primers used in qPCR and junction analysis

Primer name	Forward	Reverse
Sμ-Sγ1 junction first round	F:5-AACTCTCCAGCCACAGTAATGACC-3	R: 5- CTGTAACCTACCCAGGAGATC-3
Sμ-Sγ1 junction Second round	F:5- GCTTGAGCCAAAATGAAGTAGACT-3	R: 5- CCCCCATCCTGTCACCTATA-3
Sμ spliced	F: 5-CCCAGACCTGGGAATGTATG-3	R: 5-GGAAGACATTTGGGAAGGACT-3
Sγ1 spliced	F: 5-GGCCCTTCCAGATCTTTGAG-3	R: 5-ATGGAGTTAGTTTGGGCAGCA-3
Sμ unspliced	F: 5- TGACAGGAGGCAAGAAGACA-3	R: 5- GGGAAGACATTTGGGAAGGA-3
Sγ1 unspliced	F: 5-AAGGTTTGGTCCTGTCCTGTCC-3	R: 5-AGATGGGGGTGTCGTTTTGG-3
CD79b	F: 5-TGGTGCTGTCTTCCATGC-3	R: 5-TTGCTGGTACCGGCTCAC-3
Eμ	F: 5-CCGATCAGAACCAGAACACC-3	R: 5- GCTGGACAGAGTGTTTCAAAAC-3
Smu	F: 5-TGTAATGAACTGGAATGAGCTG-3	R: 5- CAGTCCAGTGTAGGCAGTAGAG-3
Sγ1	F: 5-GAGGAGTGCAGGAAGTCTGG-3	R: 5- CCTTGATGCCCTCCCTTT-3
Sγ3	F: 5- GGAGAAAGGAGCATAAGGAGTC-3	R: 5- GTACTTCACACCCTCACCTAC-3
AID-RT	F: 5-TGGAGACCGATATGGACAGC-3	R: 5-GGAGGTGGCACTATCTCTCC-3
GAPDH	F: 5-CACCTTCAGCTTTCCGGCCACTTAC-3	R: 5-GGAAGCCCATCACCATCTTCCAGGA-3